This article is made available via the ACS COVID-19 subset for unrestricted RESEARCH re-use and analyses in any form or by any means with acknowledgement of the original source. These permissions are granted for the duration of the World Health Organization (WHO) declaration of COVID-19 as a global pandemic.

ACSNANO

www.acsnano.org

ARTICLE

Polymersomes as Stable Nanocarriers for a Highly Immunogenic and Durable SARS-CoV-2 Spike Protein Subunit Vaccine

Jian Hang Lam, Amit K. Khan, Thomas A. Cornell, Teck Wan Chia, Regine J. Dress, Wen Wang William Yeow, Nur Khairiah Mohd-Ismail, Shrinivas Venkataraman, Kim Tien Ng, Yee-Joo Tan, Danielle E. Anderson, Florent Ginhoux, and Madhavan Nallani*

Cite This: *ACS Nano* 2021, 15, 15754–15770

Read Online

ACCESS | Metrics & More | Article Recommendations | Supporting Information

ABSTRACT: **Multiple successful vaccines against severe acute respiratory syndrome coronavirus 2 (SARS-CoV-2) are urgently needed to address the ongoing coronavirus disease 2019 (Covid-19) pandemic. In the present work, we describe a subunit vaccine based on the SARS-CoV-2 spike protein coadministered with CpG adjuvant. To enhance the immunogenicity of our formulation, both antigen and adjuvant were encapsulated with our proprietary artificial cell membrane (ACM) polymersome technology. Structurally, ACM polymersomes are self-assembling nanoscale vesicles made up of an amphiphilic block copolymer comprising poly(butadiene)-*b*-poly(ethylene glycol) and a cationic lipid, 1,2-dioleoyl-3-trimethylammonium-propane. Functionally, ACM polymersomes serve as delivery vehicles that are efficiently taken up by dendritic cells (DC1 and DC2), which are key initiators of the adaptive immune response. Two doses of our formulation elicit robust neutralizing antibody titers in C57BL/6 mice that persist at least 40 days. Furthermore, we confirm the presence of functional memory CD4$^+$ and CD8$^+$ T cells that produce T helper type 1 cytokines. This study is an important step toward the development of an efficacious vaccine in humans.**

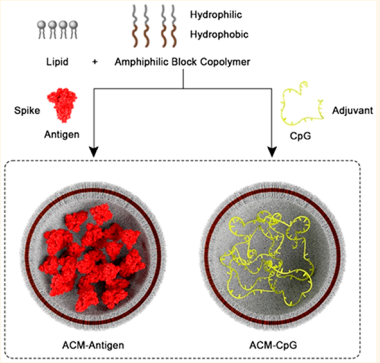

KEYWORDS: *ACM, polymersome, Covid-19, spike, vaccine, neutralizing antibody*

Vaccines are an integral part of the global healthcare strategy and have played a decisive role in eliminating or controlling numerous infectious diseases. Since Covid-19 emerged as a pandemic, rapid development of a vaccine has become a paramount focus across the globe. The etiological agent, SARS-CoV-2, is capable of efficient human-to-human transmission,[1−3] with ∼20% of patients exhibiting severe (respiratory distress) to critical (respiratory failure, septic shock, and/or multiorgan failure) symptoms.[4] SARS-CoV-2 belongs to the genus *Betacoronavirus* within the family Coronaviridae.[5] Each virion consists of a nucleocapsid protein-encapsulated single-stranded genomic ribonucleic acid (RNA), surrounded by a lipid bilayer into which spike, membrane, and envelope proteins are incorporated.[6] Trimers of spike protein form spike-like projections from the virus exterior surface and are key to host−virus interaction. The spike protein, which consists of subunits S1 and S2, enables viral entry into the host cell through the interaction of the receptor-binding domain (RBD; situated within the S1 subunit) with the angiotensin-converting enzyme 2 (ACE2) receptor of the host cell membrane. This stimulates cleavage at the S1−S2 junction by host cell proteases and induces significant structural rearrangement that exposes the hydrophobic fusion peptide, thus permitting the merging of viral and host cell membranes leading to viral entry.[7] The spike protein is immunogenic and the target of antibodies as well as T cells, particularly CD4$^+$ T cells.[8−10] Therefore, it has emerged as the key target for subunit vaccines of various modalities.

Meeting the global demand for a Covid-19 vaccine using traditional approaches of inactivated or live attenuated virus is challenging due to the requirement for a biosafety level 3 (BSL3) facility to handle SARS-CoV-2. Subunit vaccines based on the spike protein eliminate the need for handling live virus and are key to addressing the global demand challenge. Advances in structural biology and development of specialized carriers for

Received: February 9, 2021
Accepted: September 30, 2021
Published: October 7, 2021

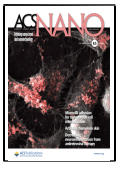

Downloaded via NATL UNIV OF SINGAPORE on February 19, 2022 at 07:00:12 (UTC).
See https://pubs.acs.org/sharingguidelines for options on how to legitimately share published articles.

© 2021 American Chemical Society

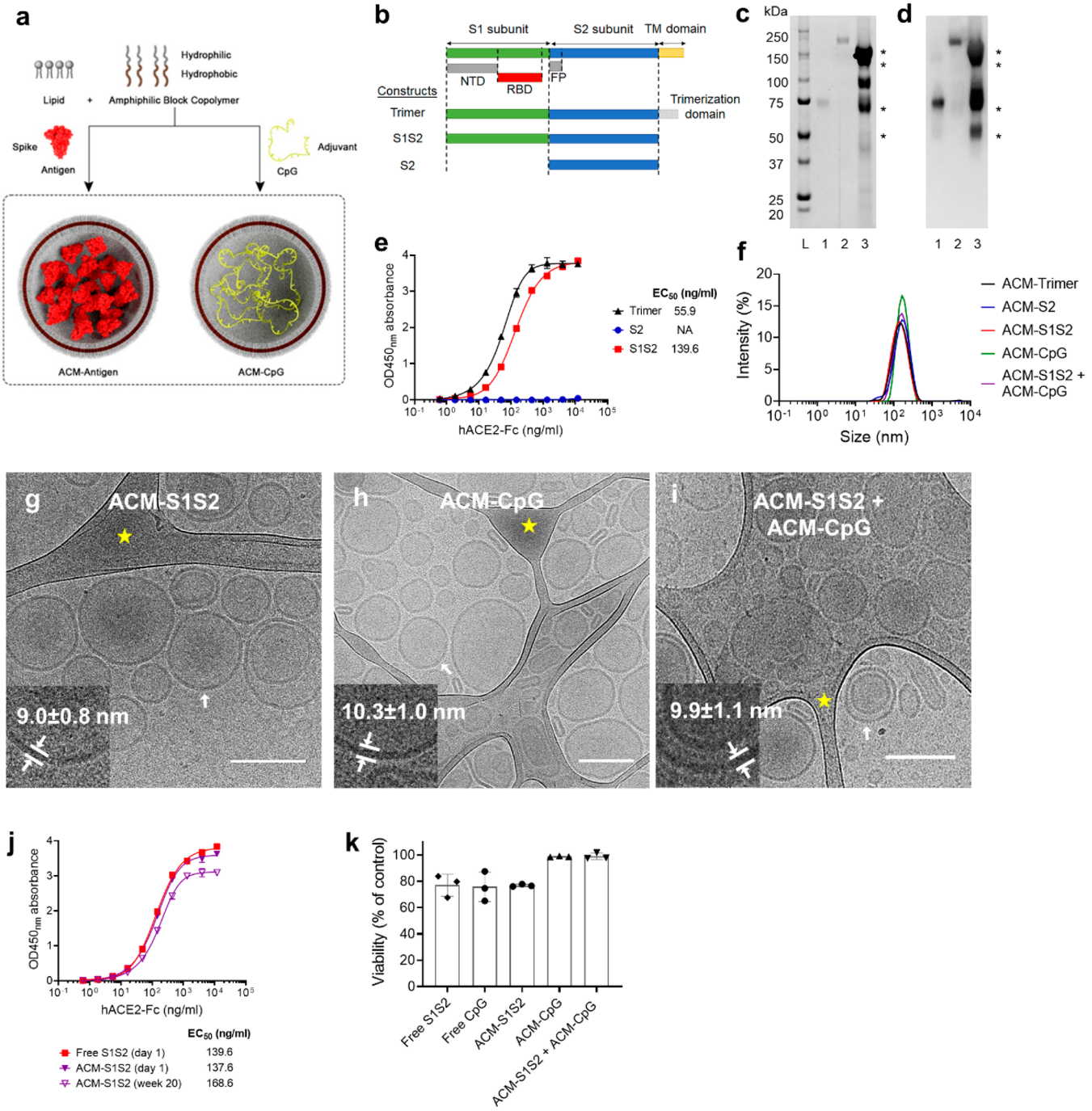

Figure 1. Preparation of ACM Covid-19 vaccine. (a) Schematic illustration of ACM-vaccine preparation. (b) Schematic of the spike protein variants used in this study. NTD: N-terminal domain. RBD: receptor-binding domain. FP: fusion peptide. TM: transmembrane. (c) SYPRO Ruby total protein stain. Lane L: Precision Plus Protein Standards (Bio-Rad). Lane 1: S2. Lane 2: trimer. Lane 3: S1S2. (d) Western blot showing antibody-reactive S1S2 bands, indicated by *. (e) ACE2-binding curves of trimer, S2, and S1S2 proteins. (f) Dynamic light scattering (DLS) measurements of ACM-antigens (ACM-trimer, ACM-S2, and ACM-S1S2) and ACM-CpG. (g–i) Cryo-EM images of ACM-S1S2, ACM-CpG, and a mixture of ACM-S1S2 + ACM-CpG illustrate the vesicular architecture with an average diameter of 158 ± 25 nm (scale bar 200 nm). Insers (lower left of each image) are magnifications of the bilayer membrane of vesicles at regions indicated by white arrows. Areas highlighted by a yellow star are lacy carbon. (j) ACE2-binding activity of encapsulated S1S2 on day 1 and after 20 weeks of storage at 4 °C. S1S2 was released *via* Triton-X 100 lysis of ACM vesicles. (k) *In vitro* cytotoxicity assay. HEK293T cells were seeded in triplicates in a 96-well plate at a density of 40 000 per well and incubated with 37.5 μg/mL of each of the following: free S1S2, free CpG, ACM-S1S2, ACM-CpG, and ACM-S1S2 + ACM-CpG. Cell viability was determined using the MTT assay against medium-only control wells.

respective cargoes (including messenger ribonucleic acid [mRNA] and protein), coupled with the rapid dissemination of the SARS-CoV-2 genomic sequence, have greatly accelerated the development of subunit vaccines. By July 2021, there were 18 vaccines approved for emergency use by at least one regulatory authority.[11] Nevertheless, some of the leading vaccine candidates do possess significant limitations. Adenoviral vectors could trigger antivector responses that may reduce the efficacy of

https://doi.org/10.1021/acsnano.1c01243
ACS Nano 2021, 15, 15754–15770

subsequent administrations.[12] mRNA vaccines formulated in lipid nanoparticles have enabled a swift response to the Covid-19 pandemic but issues of stability (currently mitigated by an ultracold chain to preserve mRNA integrity) and cost pose a major hurdle for effective and equitable distribution of such vaccines.[13]

Advancement in nanotechnology can potentially contribute to the development of a safe, cost-effective, and scalable vaccine platform, thus addressing some of the issues with the current Covid-19 vaccine candidates. Amphiphilic block copolymer self-assembly offers a straightforward, scalable route to well-defined nanoscale vesicles. By controlling the ratio of the different constituent blocks, self-assembly can be tailored to access different nanostructures, including polymersomes. The ability to compartmentalize antigens and adjuvants in the aqueous compartment of polymersomes renders them very attractive for vaccine application.[14] Compared to liposomes, polymersomes have the advantage of tuning membrane thickness and property.[15] Owing to their relatively long hydrophobic segments,[16,17] polymersomes possess enhanced stability without the need for additional stabilization strategies such as cross-linking chemistries.[18] Despite their tremendous potential, only a few reports are available employing polymersomes as a carrier for vaccine application.[19−21] Nevertheless, these limited studies clearly demonstrate that antigen-loaded polymersomes can target dendritic cells (DCs), the most efficient of antigen-presenting cells. Moreover, many polymersome attributes, such as size and surface properties, can be customized[17] to modulate their specific uptake by DCs, hence rendering polymersomes as an ideal platform for the delivery of subunit vaccines.

In the present work, we describe the development of a subunit vaccine based on the spike protein of SARS-CoV-2, coadministered with CpG adjuvant. We can encapsulate different classes of biomolecules (*i.e.*, deoxyribonucleic acid[DNA] and protein) within our proprietary artificial cell membrane (ACM) polymersomes to produce coherent and immunogenic particles, thus demonstrating the flexibility of this technology. Structurally, ACM polymersomes are self-assembling vesicles made of an amphiphilic block copolymer comprising poly(butadiene)-*b*-poly(ethylene glycol) (PBD-*b*-PEO) and a cationic lipid, 1,2-dioleoyl-3-trimethylammonium-propane (DOTAP).[22] We show here that, functionally, ACM polymersomes serve as delivery vehicles, which are efficiently taken up by DC1 and DC2, which are key initiators of the adaptive immune response. We further investigate the immunological effect of ACM polymersomes on different SARS-CoV-2 spike proteins, namely, the ectodomain of the spike protein, the S2 domain only, and a trimeric spike protein. Altogether, we show that our vaccine formulation possesses strong immunogenicity and can elicit robust and durable humoral and cellular immunity against SARS-CoV-2 in C57BL/6 mice that persist for at least 40 days.

RESULTS AND DISCUSSION

Spike Protein Purification and Encapsulation in ACM Polymersomes. The SARS-CoV-2 spike protein is immunogenic and targeted by T cells and strongly neutralizing antibodies,[8−10] making it a highly attractive subunit vaccine target. On the basis of previous work with various viral and cancer antigens (data not shown), we established that immunogenicity of a protein could be significantly improved through encapsulation within ACM polymersomes. Moreover, a further increase in the immune response could be achieved *via* coadministration of an appropriate adjuvant, such as the Toll-like receptor 9 (TLR9) agonist CpG. Therefore, our present approach involved the encapsulation of both the spike protein and the CpG adjuvant for coadministration (Figure 1a).

Given the natural configuration of the SARS-CoV-2 spike as a trimer, immunizing with a trimeric spike would be expected to generate conformationally relevant antibodies. The caveat of this approach was the requirement for a trimerization domain, typically the T4 fibritin sequence,[23] which had no regulatory precedence and may be met with substantial hurdles prior to approval. Moreover, the use of native trimeric spike protein requires an extensive purification protocol to isolate it from the host cells.[24,25] The selection of a full-length spike monomer as the vaccine candidate, rather than the S1 domain alone, was based on available evidence suggesting that a broader immune response could be elicited by the full-length protein. S1 was an obvious candidate since the RBD and N-terminal domain (NTD) were targeted by many human neutralizing antibodies.[26−29] Nevertheless, a linear neutralizing epitope was identified in the fusion peptide of the S2 domain.[30] At the same time, the potential importance of T cells should not be overlooked, given that some convalescent patients could mount a robust T cell response despite the absence of antibodies.[31] Human T cell epitopes have been mapped to both S1 and S2 domains of the spike protein.[32] In view of the existing immunogenicity data, we considered it prudent to select the ectodomain (S1S2) of the spike protein instead of S1 alone.

To generate the spike protein, we engineered T.ni cells to express a spike variant that retained S1 and S2 domains but excluded the hydrophobic transmembrane domain (hereby referred to as "S1S2"; Figure 1b), thereby improving protein solubility. In addition, we purchased an S2 fragment and a trimeric spike protein (Figure 1b) from commercial vendors to serve as controls for the subsequent immunogenicity study. S2 was ideal as a negative control since it lacked strongly neutralizing epitopes, whereas trimeric spike was used as a positive control given that it best represented the natural configuration of this viral protein.

The three spike variants were analyzed by sodium dodecyl sulfate-polyacrylamide gel electrophoresis (SDS-PAGE) followed by SYPRO Ruby staining (Figure 1c) and Western blot using mouse immune serum raised against a recombinant SARS-CoV-2 spike protein purchased from Sino Biological (Figure 1d). Total protein staining using SYPRO dye showed the S1S2 protein to consist of several bands, including two closely migrating major bands at the 150 kDa position, as well as two smaller bands at 75 and 50 kDa (Figure 1c). All four bands were recognized by spike-specific antibodies in Western blot (Figure 1d), confirming that they were all or parts of the spike protein. Among the two bands at the 150 kDa position, the heavier one corresponded to a highly glycosylated full-length spike protein, whereas the lighter one was presumed to have a lighter glycosylation profile. The remaining two Western blot-reactive bands were likely truncations of the full-length protein. The purity of our S1S2 protein was determined to be 77.0% by densitometry, and the concentration was 365 μg/mL by comparing against bovine serum albumin (BSA) standards. Interestingly, analytical size exclusion chromatography data indicated that our S1S2 protein could form higher order structures (311 kDa; Supplementary Figure 1). This was larger than an expected monomer (180 kDa[33]) and may suggest the presence of oligomers despite the absence of a trimerization domain. Functionally, our S1S2 protein bound ACE2 strongly

https://doi.org/10.1021/acsnano.1c01243
ACS Nano 2021, 15, 15754−15770

with an EC_{50} value of 139.6 ng/mL (Figure 1e) although its avidity was lower compared to the trimeric spike.

Taken together, our data suggest a correctly folded spike protein that presents a functional RBD. Adopting the correct conformation is fundamentally important from an immunization standpoint since potently neutralizing antibodies typically target the RBD,[9] although other regions of the spike protein have also been reported.[8,9,30] In the scenario where vaccination is done using an incorrectly folded protein, induction of a high ratio of binding to neutralizing antibody is expected and may predispose the individual to antibody-dependent enhancement (ADE) or vaccine-associated enhanced respiratory disease (VAERD) during actual infection.[34] ADE describes a scenario in which binding but non-neutralizing antibodies facilitate viral entry into cells bearing Fcγ receptors, notably cells of the myeloid lineage, resulting in increased viral load and disease severity.[35] With regard to VAERD, this refers to a situation wherein high levels of non-neutralizing antibodies cause excessive immune complex deposition, complement activation, and, ultimately, airway inflammation.[36,37] Although both phenomena remain theoretical possibilities in the context of Covid-19, they still argue strongly for a conformationally correct spike protein to enhance vaccine safety and efficacy.

ACM polymersomes are self-assembled from an amphiphilic block copolymer comprising PBD-*b*-PEO and the cationic lipid DOTAP.[22] When amphiphilic block copolymers encounter water, they undergo self-assembly into a thermodynamically stable bilayer conformation placing the PBD block on the inside to minimize the water interaction, whereas the water-soluble PEG block is surface-exposed. During the self-assembly process, solutes are entrapped in the vesicular cavity. DOTAP, or other charged lipids, can be used to increase electrostatic interactions to enhance encapsulation of negatively charged molecules, such as antigens and adjuvants. In this work, viral antigens (spike trimer, S2, and S1S2 protein) and CpG adjuvant were separately encapsulated in individual vesicles as ACM-trimer, ACM-S2, ACM-S1S2, and ACM-CpG, respectively. Vesicles were extruded to within a 100−200 nm diameter range followed by dialysis to remove the solvent, nonencapsulated antigens, and adjuvant. The final vaccine formulation was a 50:50 v/v mixture of ACM-S1S2 and ACM-CpG prior to administration. All samples tested negative for endotoxin using the colorimetric HEK Blue cell-based assay (Supplementary Figure 2).

The sizes and morphologies of ACM-antigen and ACM-CpG were assessed by dynamic light scattering (DLS) and cryogenic-transmission electron microscopy (cryo-TEM), respectively. Overall, the sizes of ACM polymersomes followed a unimodal intensity-weighted distribution with a mean *z*-average hydrodynamic diameter of 158 ± 25 nm (Figure 1f). The sizes of the different ACM-antigen preparations were comparable: ACM-trimer, 133 nm (polydispersity index [PDI] 0.192); ACM-S1S2, 139 nm (PDI 0.181); and ACM-S2, 143 nm (PDI 0.178). ACM-CpG, on the other hand, was slightly larger at 183 nm (PDI 0.085). The final vaccine formulation (ACM-S1S2 + ACM-CpG) showed a size distribution comparable with those of individual vesicles (Figure 1f). Electron micrographs revealed a vesicular architecture (Figure 1g−i). From line profile measurements, the bilayer thicknesses of ACM-S1S2, ACM-CpG, and ACM-S1S2 + ACM-CpG were estimated to be 9.0 ± 0.8, 10.3 ± 1.0, and 9.9 ± 1.1 nm, respectively. Compared to liposomes with a bilayer thickness of 3−5 nm, ACM polymersomes had thicker membranes (9−10 nm), which in turn had been shown to impart better stability.[17]

To assess protein encapsulation within vesicles, ACM-antigen particles were lysed with 2.5% nonionic surfactant Triton-X 100 and then characterized by SDS-PAGE alongside free protein calibration standards. The concentrations of encapsulated proteins were quantified by the densitometric method from SDS-PAGE followed by SYPRO Ruby staining (Supplementary Figure 3a−c). ACM polymers interacted with SYPRO stain to generate a distinct smear at the bottom of the lane, and co-localization of the protein band with this smear confirmed that encapsulation had occurred. The amounts of encapsulated trimer, S1S2, and S2 were determined to be 48, 46, and 25.7 μg/mL, respectively, from 100 μg/mL starting concentrations. To remove free protein that escaped encapsulation, all ACM preparations were dialyzed. A parallel dialysis experiment with free protein control was performed to determine the quantity of free protein remaining in each ACM preparation. SYPRO staining showed 19.8 μg/mL free trimer, 7.5 μg/mL free S1S2 protein, and 0 μg/mL free S2 remaining after dialysis from 100 μg/mL starting protein concentrations (Supplementary Figure 3a−c), indicating that the majority of the nonencapsulated proteins were removed from ACM-S1S2 and ACM-S2 preparations, whereas close to 40% free protein remained with the ACM-trimer sample. The lower efficiency of trimer removal may be caused by its larger size relative to S1S2 or S2, thus reducing its diffusion across the dialysis membrane. To quantify the concentration of CpG encapsulated in ACM vesicles, the DNA-binding dye SYBR Safe was used. Based on the 530 nm fluorescent emission, the encapsulation of ACM-CpG was determined to be 480 μg/mL at an efficiency of 60%.

To determine whether ACM encapsulation had inadvertently impaired the structure and function of spike protein, S1S2 protein was released from vesicles through Triton-X 100 lysis, and its activity assessed by the ACE2-binding assay. Compared to the free protein with an EC_{50} of 139.6 ng/mL, ACM-S1S2 possessed an EC_{50} of 137.6 ng/mL (Figure 1j), indicating no alteration to its function. Given the importance of shelf life and product stability in the context of local and global distribution, we performed a stability study on free S1S2 protein, ACM-S1S2, free CpG, ACM-CpG, free S1S2 + free CpG, and ACM-S1S2 + ACM-CpG at 4 and 37 °C. The initial observation showed a very stable vesicle with no change of size and PDI of the ACM-S1S2 formulation, no degradation of S1S2 protein content, and minimal loss of activity for up to 20 weeks at 4 °C measured by DLS, SDS-PAGE followed by SYPRO staining (Supplementary Figure 4a−c), and ACE2-binding assay (Figure 1j). However, an accelerated stability study at 37 °C showed a decrease in protein concentration for both free S1S2 and ACM-S1S2 after 1 week (Supplementary Figure 5a), indicating proteolytic degradation at elevated temperature. Unexpectedly, samples containing CpG (either ACM-S1S2 + ACM-CpG or free S1S2 + free CpG) exhibited reduced protein degradation. Further, only ACM-S1S2 + ACM-CpG maintained its protein content for up to 28 days, whereas other formulations showed complete proteolysis (Supplementary Figure 5a). It remained unclear how CpG was able to maintain protein stability at 37 °C, although we speculated that the negatively charged CpG may possibly associate with proteases present as impurities in the S1S2 sample, thereby hindering proteolysis of S1S2 protein. In contrast, the size and PDI of the ACM formulations remained stable over the 28-day time course (Supplementary Figure 5b,c).

DOTAP-based nanoparticles are generally cytotoxic owing to the cationic nature of the lipid.[38] Although, we had only 30 mM of DOTAP in our polymersomes, we wanted to investigate

https://doi.org/10.1021/acsnano.1c01243
ACS Nano 2021, 15, 15754−15770

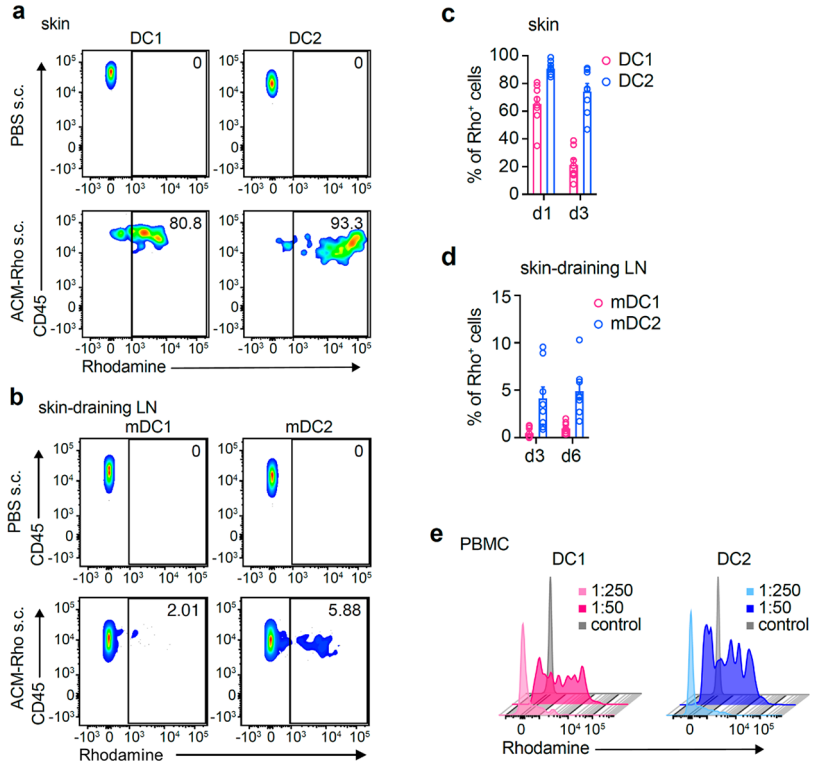

Figure 2. ACM vesicles were efficiently taken up by DCs. (a–d) Mice (n = 8) SC injected with ACM-Rhodamine vesicles. (a) Rhodamine signals from skin DC1 and DC2 1 day post-SC injection. (b) Rhodamine signals from migratory DC1 and DC2 in skin-draining LNs 6 days post-SC injection. (c, d) Graphs showing % of Rhodamine$^+$ DC1 and DC2 in skin and skin-draining LNs. (e) Rhodamine signals by DC1 and DC2 from human PBMCs after incubation with different dilutions of ACM-Rhodamine.

potential toxicity issues with our vaccine formulation. We incubated the human embryonic kidney 293T (HEK293T) cell line, frequently used for cytoxicity assessment,[39,40] with ACM-S1S2 and ACM-CpG individually or in combination and determined cell viability using the MTT assay (Figure 1k). Antigen or adjuvant was normalized to a concentration of 37.5 μg/mL, which represented the highest possible amount of material that we could apply to the assay, after considering encapsulation efficiency and assay dilution. Free S1S2 and free CpG each induced a slight drop of approximately 25% in viability. ACM-S1S2 also induced a similar loss of viability, whereas ACM-CpG did not impair viability. In combination, ACM-S1S2 and ACM-CpG also did not impair viability of HEK293T. Altogether, the data suggested that the ACM-S1S2 + ACM-CpG formulation was not cytotoxic at the concentration of 37.5 μg/mL. To further investigate potential safety issues with our vaccine formulation, preclinical animal toxicity analysis is currently ongoing.

In summary, we have expressed and purified functional SARS-CoV-2 spike ("S1S2") protein from T.ni cells that bound ACE2 with high avidity. This suggested a correctly folded protein, which was necessary for the induction of neutralizing antibodies. The protein and CpG adjuvant were separately encapsulated in ACM-polymersomes for the purpose of coadministration in our final vaccine formulation. Based on an *in vitro* cytotoxicity assay, our formulation was nontoxic at the concentration of 37.5 μg/mL. In stability tests, the ACM-encapsulated S1S2 protein quickly degraded at 37 °C but remained intact and functional for at least 20 weeks at 4 °C. With proper temperature control at 4 °C during storage, transport, and distribution, our ACM-S1S2 formulation would be expected to maintain functionality for prolonged periods.

ACMs Are Efficiently Taken up by DCs. To gain long-lasting immunity against viruses, such as SARS-CoV-2, the initial induction of an efficient immune response is crucial. DCs, which can be roughly divided into XCR1/CD8/CD103$^+$CD11b$^-$ classical DC1 and CD11b$^+$XCR1/CD8/CD103$^-$ classical DC2,[41,42] are cells of the innate immune system highly specialized in priming and activation of naïve CD8$^+$ T cells and CD4$^+$ T cells. Following the uptake of foreign antigens, DCs process and present them to naïve CD8$^+$ T cells or CD4$^+$ T cells *via* their MHC-I or MHC-II complexes, resulting in antigen-specific cytotoxic and helper T cell responses, respectively.[42,43]

To analyze the capacity of DCs to take up ACM polymersomes, mice were injected subcutaneously (SC) with either phosphate-buffered saline (PBS) or the nontoxic dye Rhodamine conjugated to the polymer of ACM vesicles. At 1 to 6 days postinjection, expression of Rhodamine by DCs in the skin and skin-draining lymph nodes (LNs) was examined by flow cytometry. Both DC1 and DC2 could efficiently take up ACM-Rhodamine, as evidenced by the high Rhodamine signals recorded in both cell types (Figure 2a). However, DC2 in the skin seemed to be more potent in ACM-Rhodamine uptake over time as compared to DC1, with around 80–90% of DC2 remaining Rhodamine$^+$ on days 1 to 3 postinjection compared to around 70% and 20% of DC1 on days 1 and 3, respectively (Figure 2c). While we could not detect any signal for Rhodamine in the draining LNs on day 1 postinjection (data not shown), around 2–5% of migratory DC1 (mDC1) and migratory DC2 (mDC2) had taken up ACM-Rhodamine as early as day 3 postinjection (Figure 2b,d). Collectively, these experiments show that DCs take up ACMs from the skin and then migrate to the draining LNs with their "ACM cargo". As the LNs are the prime location for DC-T cell interaction, we

https://doi.org/10.1021/acsnano.1c01243
ACS Nano 2021, 15, 15754–15770

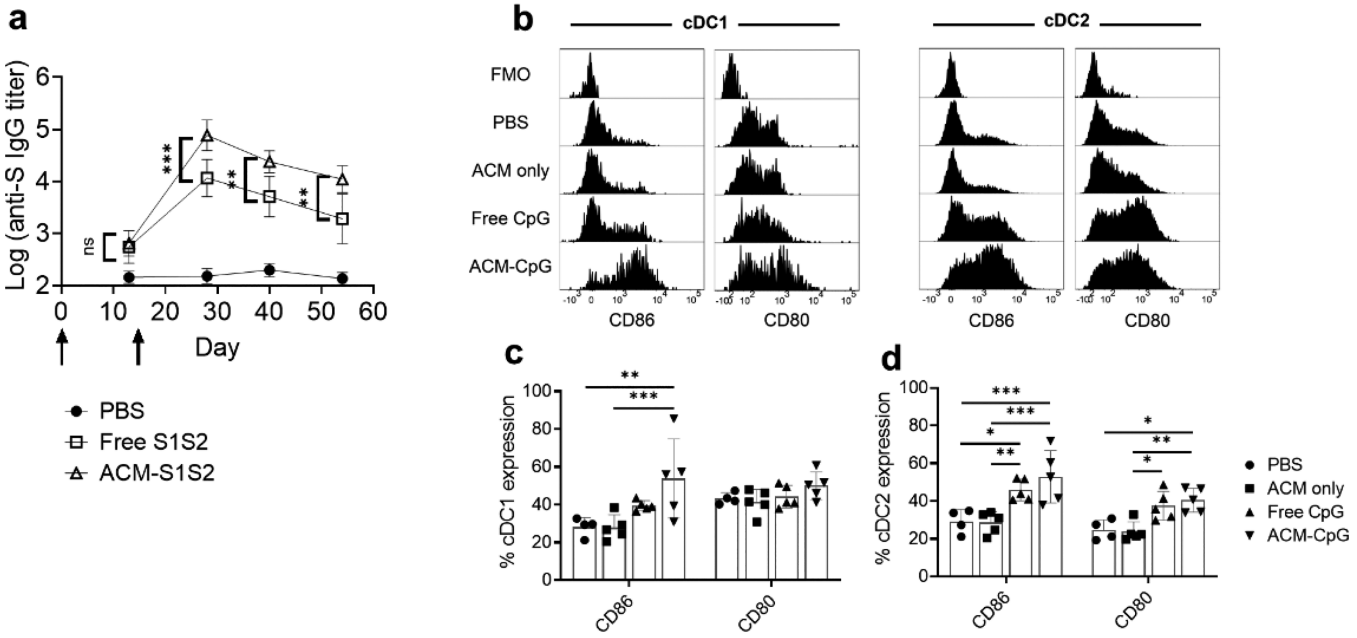

Figure 3. Immunological effects induced by *in vivo* release of ACM-S1S2 and ACM-CpG. (a) *In vivo* release of ACM-S1S2. C57BL/6 mice were SC immunized on day 0 and 14 (indicated on graph by arrows) with free or ACM-encapsulated S1S2. Serum IgG was assessed on days 13, 28, 40, and 54 as a measure of S1S2 release to induce an antigen-specific immune response. Two-way ANOVA with Tukey's multiple comparison was performed. Only comparisons between free and ACM-S1S2 are shown. (b–d) *In vivo* release of ACM-CpG. C57BL/6 mice were SC injected with one of the following: (i) PBS, (ii) ACM only, (iii) free CpG, or (iv) ACM-CpG. Inguinal LNs (draining the site of injection) were harvested 2 days later to assess activation of cDC1 and cDC2 by flow cytometry. (b) Representative histograms showing expression of the activation markers CD86 and CD80. FMO: fluorescence-minus-one staining control. (c, d) Proportions of CD86- and CD80-expressing cDC1 and cDC2 from the mouse groups with the different treatments. Two-way ANOVA with Sidak's multiple comparison was performed. Only statistically significant differences are shown.

speculate that these ACM-loaded DCs interact with naïve $CD8^+$ T cells or $CD4^+$ T cells to prime and polarize them for further responses.

To translate our results from mouse to human, we cultured primary human peripheral blood mononuclear cells (PBMCs) with ACM-Rhodamine in varying concentrations overnight and assessed their ability to take up ACM-Rhodamine by flow cytometry. We found that, compared to our mouse data, both human DC subsets, $CD141^+$ DC1 and $CD1c^+$ DC2, were capable of efficiently taking up ACM-Rhodamine, as indicated by the high expression of Rhodamine in both populations, relative to the control (Figure 2e). Since uptake was also observed in monocytes but not B or T cells (Supplementary Figure 6), this indicated a process that was dependent on cell type.

In conclusion, both DC1 and DC2 are capable of efficiently taking up ACMs and thus likely to present ACM-encapsulated antigen to naïve $CD8^+$ T cells or $CD4^+$ T cells. This may potentially induce a strong and durable adaptive immune response, which is highly desirable in the context of a vaccine.

***In Vivo* Release of ACM-S1S2 and ACM-CpG.** Next, we examined whether ACM polymersomes could release encapsulated cargo following SC administration in mice. For our initial experiments, ACM-Rhodamine was encapsulated with DQ-ovalbumin (DQ-OVA) in its vesicular cavity; the Rhodamine fluorescent signal would inform us of successful internalization of the vesicle, whereas the DQ fluorescent signal, which was generated only after cleavage by lysosomal hydrolases, would inform us of successful release of ACM cargo within the endosome. DC2 was observed to coexpress Rhodamine and DQ-OVA (Supplementary Figure 7a), indicating release of ACM cargo, although the efficiency of uptake was considerably poorer than uptake of ACM-Rhodamine alone, as evidenced by the low proportion (~30%) of cells in skin expressing Rhodamine signal (Supplementary Figure 7b). On the other hand, DC1 seemed to either have a lower take up rate or completely fail to take up ACM-Rhodamine/DQ-OVA (Supplementary Figure 7a,b). Subsequently, only approximately 0.05% of ACM-Rhodamine/DQ-OVA^+ cells were detected in LNs at the late time point of day 6 and were identified as DC2 (Supplementary Figure 7c). These results suggested that the physicochemical property of ACM-Rhodamine/DQ-OVA may be adversely altered to the detriment of DC uptake.[44] Nevertheless, we did observe a clear DQ signal from DC2, which indicated potential release of ACM cargo within DCs.

On the basis of the initial findings with ACM-Rhodamine/DQ-OVA, we proceeded to examine the *in vivo* release characteristics of our vaccine components. For ACM-S1S2, mice were SC vaccinated on days 0 and 14 with 5 μg of free or encapsulated spike protein. Antigen-specific serum immunoglobulin G (IgG) was used as an indication that S1S2 was successfully released from ACM polymersomes to elicit an immune response (Figure 3a). No antibody response was detected from PBS controls over the 54-day study period, whereas clear IgG titers were detected in all mice immunized with free or encapsulated S1S2. IgG titers peaked on day 28 after the second dose and gradually declined for the remainder of the study period but remained detectable at the final time point of day 54. Notably, levels of IgG from mice immunized with ACM-S1S2 were significantly higher than mice immunized with free S1S2 at all time points after boost, indicating that encapsulation had enhanced the immunogenicity of the spike protein.

https://doi.org/10.1021/acsnano.1c01243
ACS Nano 2021, 15, 15754–15770

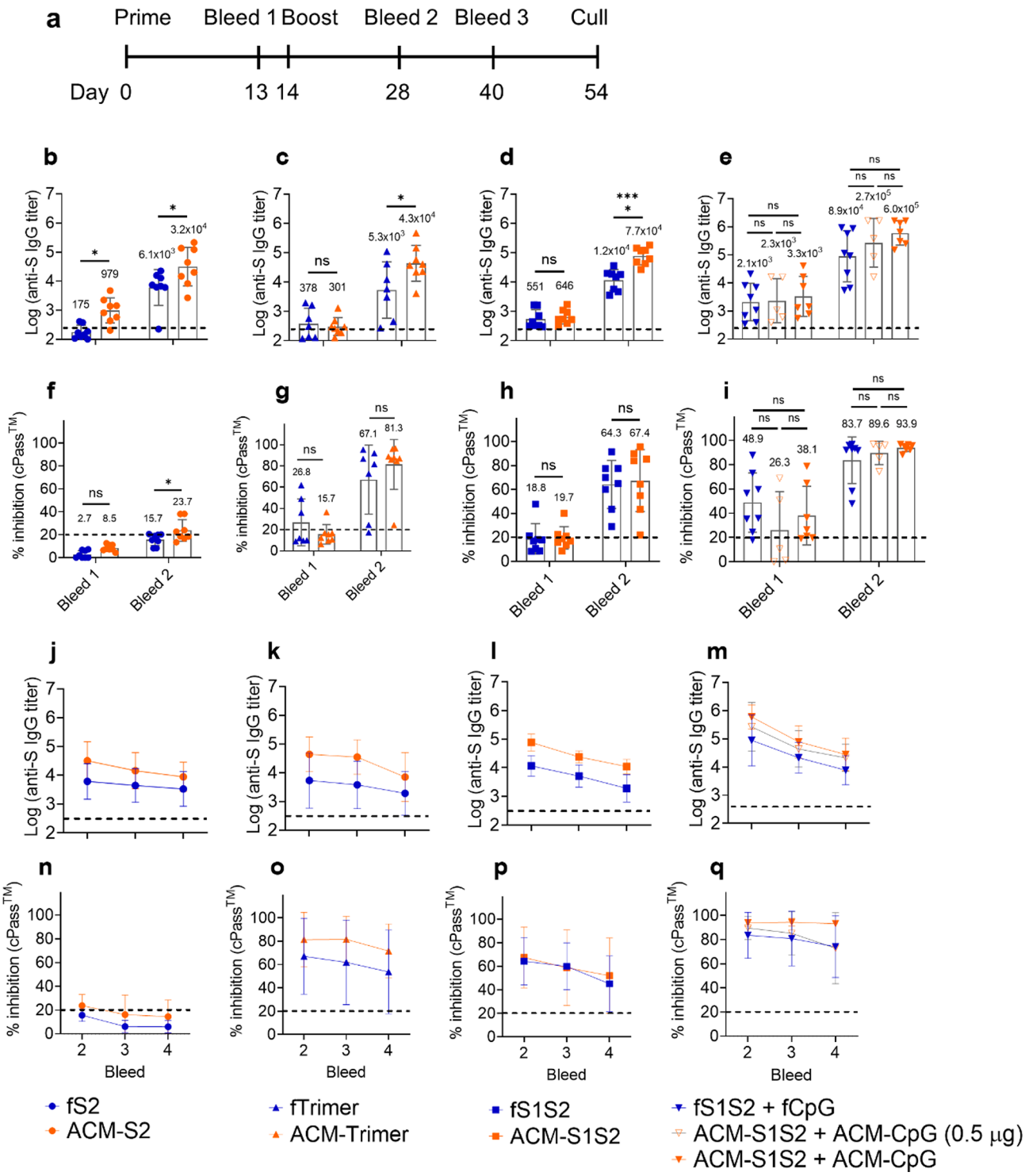

Figure 4. Antibody responses to ACM Covid-19 vaccine candidates. (a) Immunization and blood collection schedule. Each group consisted of 7−8 C57BL/6 mice, SC immunized twice with 5 μg of antigen ±5 μg CpG per dose. One group (n = 5) immunized with ACM-S1S2 + ACM-CpG received 1/10th dose (0.5 μg) as part of a limited dose-sparing study. (b−e) Spike-specific total IgG titers at bleed 1 (after prime) and bleed 2 (after boost). End point ELISA IgG titers were determined on plates coated with spike protein. GMTs are indicated above bar graphs. Horizontal dashed line denotes highest background measurement from PBS-injected mice. (b) Mice immunized with fS2 or ACM-S2. (c) fTrimer or ACM-Trimer. (d) fS1S2 or ACM-S1S2. (e) We also investigated the potential benefit of including CpG adjuvant. The following groups were examined: fS1S2 + fCpG, ACM-S1S2 + ACM-CpG, and ACM-S1S2 + ACM-CpG (0.5 μg). Two-way ANOVA with Sidak's multiple comparison was performed. *: $P \leq 0.05$; **: $P \leq 0.01$; ***: $P \leq 0.001$; ****: $P \leq 0.0001$; ns: not significant. (f−i) Surrogate virus neutralization test. Serum neutralizing activity was determined using an ELISA-based cPass kit that assessed antibodies blocking the interaction between RBD and ACE2 receptor. Arithmetic means are indicated above bar graphs. A cutoff of 20% inhibition (horizontal dashed line) was recommended by the manufacturer to define seropositive samples. Sera from mice vaccinated with S2 (f), trimer (g), S1S2 (h), and S1S2 + CpG (i). (j−q) Kinetics of spike-specific total IgG titers after boost, for vaccination with free or ACM-encapsulated S2 (j), trimer (k), S1S2 (l), or S1S2 + CpG (m), and kinetics of neutralizing activity after boost, for vaccination with free or ACM-encapsulated S2 (n), trimer (o), S1S2 (p), or S1S2 + CpG (q).

https://doi.org/10.1021/acsnano.1c01243
ACS Nano 2021, 15, 15754−15770

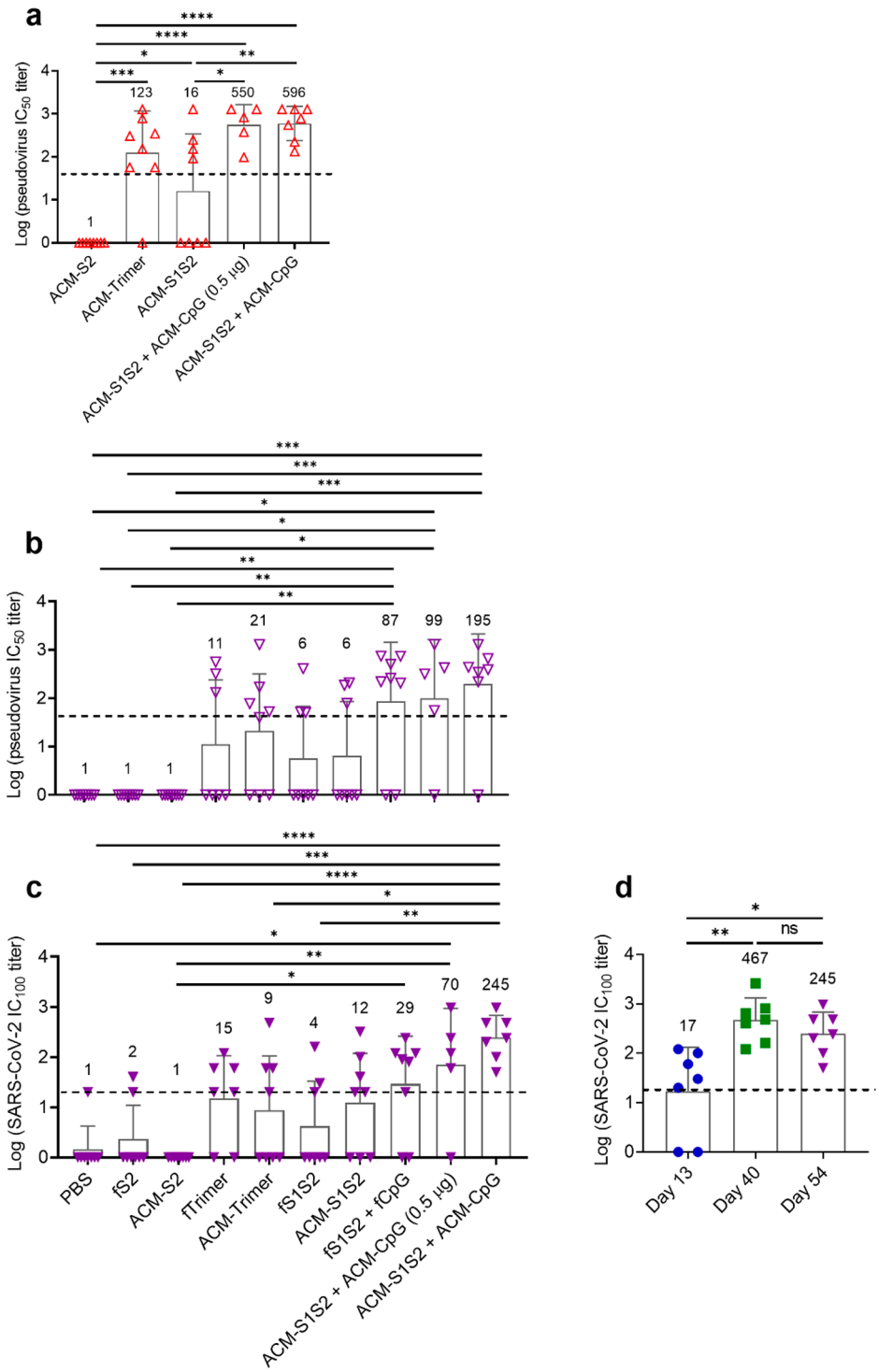

Figure 5. Virus neutralizing tests confirmed the ability of the ACM-S1S2 + ACM-CpG vaccine to induce a robust, durable neutralizing response. (a) Day 28 sera (representing the time point of peak response) from five key mouse groups, after vaccination with ACM-S2, ACM-Trimer, ACM-S1S2, and ACM-S1S2 + ACM-CpG (0.5 or 5 μg). (b) IC_{50} pseudovirus neutralizing titers on day 54 (last assessed time point). (c) IC_{100} live SARS-CoV-2 neutralizing titers on day 54. (d) Kinetics of neutralizing titers from ACM-S1S2 + ACM-CpG-immunized mice. One-way ANOVA with Tukey's multiple comparison was performed; only significant differences are shown. *: $P \leq 0.05$; **: $P \leq 0.01$; ***: $P \leq 0.001$; ****: $P \leq 0.0001$. GMTs are indicated above bar graphs. Lower limits of detection are indicated by horizontal dashed lines; samples below threshold are assigned a nominal value of 1.

For ACM-CpG, mice were SC injected with a single dose of 5 μg of CpG (free or encapsulated), and cDCs in draining LNs were examined 2 days later for upregulation of activation markers (Figure 3b), as a readout for successful release. We found similar expression of the activation markers CD80 and CD86 on cDC1 and cDC2 after treatment with empty ACMs or PBS (Figure 3c,d), indicating that polymersomes were intrinsically nonimmunogenic and failed to activate DCs. Mice treated with free CpG exhibited significant increases in CD86 and CD80 expression on cDC2 (Figure 3d) but not cDC1 (Figure

https://doi.org/10.1021/acsnano.1c01243
ACS Nano 2021, 15, 15754−15770

3c), compared to PBS- or empty ACM-injected mice. In contrast, cDC1 from ACM-CpG-injected mice exhibited a highly significant increase in CD86 expression compared to PBS- or empty ACM-injected mice (Figure 3c), whereas cDC2 showed highly significant increase in expression of both CD86 and CD80 (Figure 3d). Although the difference between free CpG- and ACM-CpG-treated mice remained nonsignificant, the results clearly showed the effect of free CpG to be restricted to cDC2, whereas ACM-CpG could strongly activate both DC subsets. Collectively, these *in vivo* data demonstrated superior DC activation by ACM-CpG, despite the lack of intrinsic immunogenicity of empty ACM polymersomes, suggesting that the immune-enhancing effect of ACM was due to efficient delivery of their cargo to DCs. Moreover, the results supported the use of ACM-S1S2 and ACM-CpG in combination to capitalize on their respective benefits.

ACM-S1S2 + ACM-CpG Formulation Induced Robust and Durable Neutralizing Antibodies against SARS-CoV-2 in Mice. A total of nine vaccine formulations underwent immunological assessment in C57BL/6 mice. Two doses of each formulation were administered at a 2-week interval via SC injection, and serum antibodies were examined on day 13 (preboost) and days 28, 40, and 54 (postboost) (Figure 4a). All antigens were injected at 5 μg per dose with or without 5 μg of CpG adjuvant. Antigen dose was selected based on the prior scientific report,[45] whereas the dose of CpG was based on the amount frequently described in mouse vaccination experiments.[46−48] Additionally, one group of mice received the ACM-S1S2 + ACM-CpG formulation at 1/10th dose (0.5 μg) for a limited dose-sparing investigation, based on an earlier report that 10-fold reduction of CpG remained efficacious when delivered by nanoparticles.[48] IgG titers against spike protein were higher at day 28 as compared to day 13, indicating a boost effect. Immunization with ACM-S2 gave significantly higher IgG titers as compared to free S2 (fS2; Figure 4b), significantly higher with ACM-trimer as compared to free trimer (fTrimer; Figure 4c) and significantly higher with ACM-S1S2 as compared to free S1S2 (fS1S2; Figure 4d). These data suggested that ACM encapsulation improved immunogenicity of each antigen. Moreover, we showed earlier that ACM encapsulation of CpG resulted in superior DC activation compared to free CpG. Taken together, these results strongly supported the use of ACM-S1S2 and ACM-CpG in combination. Among mice immunized with free S1S2 + free CpG (fS1S2 + fCpG), ACM-S1S2 + ACM-CpG, or ACM-S1S2 + ACM-CpG (0.5 μg), similarly high titers were obtained after two doses (Figure 4e). Nevertheless, ACM encapsulation of S1S2 + CpG resulted in a slight but nonsignificant titer increase, which was also characterized by tight clustering of data points indicative of greater consistency in the immune response (Figure 4e).

To further investigate the potential of protective immunity of these vaccine candidates, we performed a surrogate virus neutralization assay (cPass kit) as described in Materials and Methods. Vaccination with S2 induced little to no neutralizing antibodies (Figure 4f), consistent with the absence of neutralizing epitopes in this domain. For trimer or S1S2, widely varying neutralizing activities ranging from <20% to >95% inhibition were detected at day 28 for either free or ACM-encapsulated antigens (Figure 4g,h). For fS1S2 + fCpG, good neutralizing activity was detected in 6/8 mice (>90% inhibition) and moderate activity (<60% inhibition) in 2/8 mice. For ACM-S1S2 + ACM-CpG, strong neutralizing activity was consistently detected in all mice (88.4−96.8% inhibition). Notably, even the 1/10th dose was highly efficacious (74.4−96.8% inhibition) (Figure 4i). Collectively, the cPass data suggested that coadministering ACM-encapsulated spike protein and CpG facilitated the development of uniformly strong immune responses, whereas coadministering free spike protein and free CpG did not.

To monitor antibody kinetics, further samples were taken on day 40 (bleed 3) and day 54 (bleed 4). A gradual decline in spike-specific total IgG titers was seen in mice administered with free or ACM-encapsulated S2, trimer, S1S2, or S1S2 + CpG (Figure 4j,k,l,m). Kinetics were also determined for neutralizing antibodies measured by the cPass kit. Concomitant with the respective IgG profiles, there was a gradual decline of the neutralizing antibodies from mice vaccinated with free or ACM-encapsulated S2, trimer, or S1S2 (Figure 4n,o,p). With regard to S1S2 + CpG, the free antigen and free CpG formulation showed a progressive decline in neutralizing activity, whereas ACM-S1S2 + ACM-CpG maintained neutralizing antibodies at high levels between days 28 and 54 (average of 93.9 ± 3.0%, 94.5 ± 3.2%, and 93.3 ± 2.7% inhibition on days 28, 40, and 54, respectively), despite falling IgG titers. Durability in antibody response was, however, lost when the dose was reduced to 1/10th (Figure 4q). Altogether, the data here suggested that the ACM-S1S2 + ACM-CpG formulation at 5 μg dose was able to induce uniformly high neutralizing responses that were durable for at least 40 days after the final administration.

To confirm these findings, we performed a pseudovirus neutralization test on day-28 sera from five key groups: ACM-S2, ACM-trimer, ACM-S1S2, and ACM-S1S2 + ACM-CpG (0.5 μg and 5 μg dosage groups). As expected, ACM-S2 failed to generate neutralizing antibodies against SARS-CoV-2 spike-pseudotyped virus (IC_{50} titer <40; Figure 5a). For the ACM-trimer and ACM-S1S2 mouse groups, partial seroconversion was observed with 7/8 and 4/8 mice, respectively, showing a positive response (IC_{50} titer ≥40). Finally, the ACM-S1S2 + ACM-CpG mouse group showed complete seroconversion at high titers (geometric mean titer [GMT] of 596; Figure 5a). Interestingly, even the 1/10th (0.5 μg) dose remained highly efficacious, eliciting seroconversion in 5/5 mice with a GMT of 550.

We proceeded to analyze sera from the last time point (day 54) by pseudovirus and live SARS-CoV-2 neutralization tests (Figure 5b,c). Neutralizing responses across mouse groups were generally moderate to low, with many mice falling below respective limits of detection. Only the ACM-S1S2 + ACM-CpG (5 μg dose) group retained high neutralizing titers against pseudovirus (GMT of 195; Figure 5b) and live SARS-CoV-2 (GMT of 245; Figure 5c). Statistical analysis indicated ACM-S1S2 + ACM-CpG induced significantly higher GMT compared to PBS, fS2, ACM-S2, ACM-Trimer, and fS1S2. Even though the difference with the 1/10th dose was not significant, the GMT of the 1/10th dose was reduced 2.0-fold against pseudovirus and 3.5-fold against SARS-CoV-2, suggesting loss of efficacy at this late time point with dose reduction. Between the two neutralizing assays, results were generally in strong agreement (Pearson correlation coefficient: 0.83; Supplementary Figure 8) although some discrepancies were observed. In particular, we noticed one mouse from the ACM-S1S2 + ACM-CpG group that was seemingly seronegative on day 54 by a pseudovirus neutralization test but was consistently seropositive across time points by the cPass assay as well as live the SARS-CoV-2 neutralization test. This discrepancy may arise from the relatively high threshold of 1:40 serum dilution of the

https://doi.org/10.1021/acsnano.1c01243
ACS Nano 2021, 15, 15754−15770

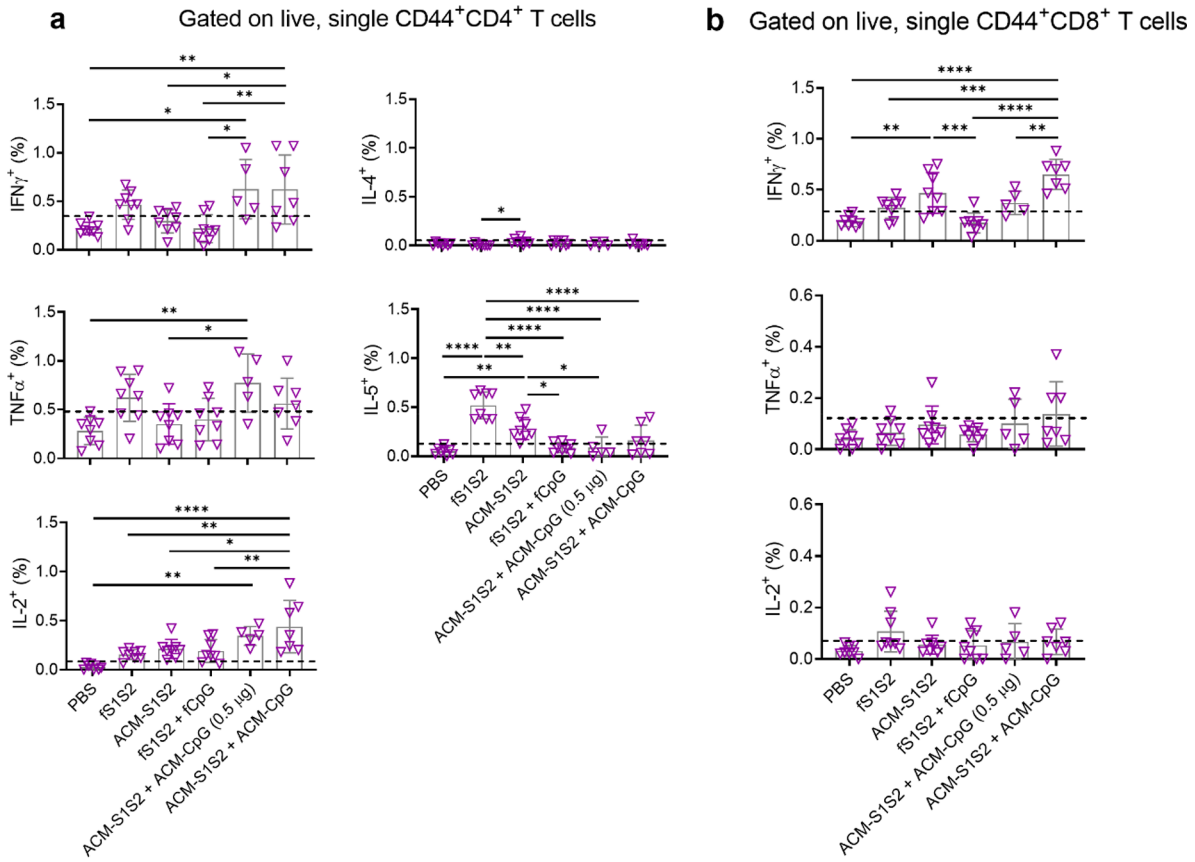

Figure 6. | ACM-S1S2 + ACM-CpG vaccine elicited functional memory CD4$^+$ and CD8$^+$ T cells. Spleens were harvested on day 54 (40 days after boost), and splenocytes (including those from PBS controls) were stimulated *ex vivo* with an overlapping peptide pool covering the SARS-CoV-2 spike protein. T cell responses were determined by intracellular cytokine staining. (a) Th1 (IFNγ, TNFα, and IL-2) and Th2 (IL-4 and IL-5) cytokine production by CD44^{hi}CD4$^+$ T cells. (b) IFNγ, TNFα, and IL-2 production by CD44^{hi}CD8$^+$ T cells. Baselines were assigned according to PBS controls, and readings above them were considered antigen-specific. One-way ANOVA with Tukey's multiple comparison was performed; only significant differences are shown. *: $P \leq 0.05$; **: $P \leq 0.01$; ***: $P \leq 0.001$; ****: $P \leq 0.0001$.

pseudovirus assay, which was needed to address high background activity of some naïve mice that we and others[49] have noticed. At the same time, we must acknowledge that our understanding of the SARS-CoV-2 infection process is likely incomplete. The design of the pseudovirus virus assay is based on the interactions between SARS-CoV-2 spike protein and host cell ACE2 receptor and proteases,[50,51] as well as the ability of neutralizing antibodies to disrupt these interactions.[52] It is possible that antibodies may neutralize in a mechanism not recapitulated by this assay. Therefore, results should be validated with a live SARS-CoV-2 neutralization test, which is the gold standard.

To better understand the kinetics of the neutralizing response after ACM-S1S2 + ACM-CpG (5 μg dose) vaccination, sera from days 13 and 40 were also assessed by the live virus neutralization test (Figure 5d; day 28 sera unavailable due to the earlier pseudovirus test). A single dose of ACM-S1S2 + ACM-CpG elicited partial seroconversion with a GMT of 17 on day 13, whereas two doses resulted in a sharp rise in GMT to 467 on day 40, followed by a slight but nonsignificant drop to 245 on day 54. Together with the earlier serum IgG data, this strongly supported a prime-boost regimen to induce robust neutralizing titers. Altogether, we demonstrated that ACM-S1S2 + ACM-CpG at a 5 μg dose induced high levels of neutralizing antibodies in all mice. Moreover, neutralizing titers persisted at least 40 days after the last administration, suggesting a durable response.

ACM-S1S2 + ACM-CpG Formulation Induced T Helper Type 1 (Th1)-Biased, Functional Memory T Cells against SARS-CoV-2 Spike Protein in Mice. To evaluate spike-specific T cell responses, splenocytes were harvested from all mice on day 54 and stimulated *ex vivo* with an overlapping peptide pool covering the spike protein. T cell function was measured by intracellular cytokine staining. At this late time point (40 days after boost), activated T cells would have progressed beyond the initial expansion phase and entered contraction/memory phase.[53] To the best of our knowledge, only one mRNA vaccine had been investigated for murine T cell responses at the late time point of 7 weeks after boost.[54] Memory-phenotype CD4$^+$ and CD8$^+$ T cells were identified by gating on the respective CD44^{hi} subpopulations (Supplementary Figure 9a). Among the S1S2 vaccine groups, only the ACM-S1S2 + ACM-CpG formulation (5 μg dose) induced significant increase in interferon gamma (IFNγ)-, tumor necrosis factor alpha (TNFα)-, or interleukin-2 (IL-2)-expressing CD4$^+$ T cells, compared to PBS, fS1S2, ACM-S1S2, or fS12 + fCpG (Figure 6a and Supplementary Figure 9b). For the S2 and trimer mouse groups, no significant increase in Th1 cytokine-producing CD4$^+$ T cells was detected above baseline (Supplementary Figure 9d). With regard to T helper type 2 (Th2) cytokines, interleukin-4 (IL-4) was not detected in any mouse group, whereas interleukin-5 (IL-5) was consistently elevated in nonadjuvanted S1S2-, S2-, or trimer-immunized mice (Figure 6a and

https://doi.org/10.1021/acsnano.1c01243
ACS Nano 2021, 15, 15754−15770

Supplementary Figure 9d, respectively), indicating a Th2-biased immune response. Strikingly, production of IL-5 was strongly suppressed by coadministration of CpG. In particular, the ACM-S1S2 + ACM-CpG formulation (5 or 0.5 μg dose) produced a clear Th1-polarized profile (Figure 6a). With regard to $CD8^+$ T cells (Supplementary Figure 9c), IFNγ was the predominant response in the ACM-S1S2 + ACM-CpG (5 μg dose) group, with significantly elevated activity compared to PBS, fS1S2, fS1S2 + fCpG, or ACM-S1S2 + ACM-CpG (0.5 μg dose) (Figure 6b). Additionally, some mice had slight expression of TNFα and IL-2 although the average frequencies of responding cells were not significantly elevated. A similar cytokine profile was seen in the ACM-S1S2 group, although only 5/8 mice had IFNγ responses above baseline. For the remaining mouse groups, $CD8^+$ T cell responses were not significantly elevated (Figure 6b and Supplementary Figure 9e). Collectively, ACM-S1S2 + ACM-CpG (5 μg dose) induced in all mice functional memory $CD4^+$ and $CD8^+$ T cells that were readily detected even after 40 days from the last administration. Additionally, $CD4^+$ T cells exhibited a Th1-skewed cytokine profile.

CONCLUSIONS

ACM-SARS-CoV-2 vaccine (ACM-S1S2 + ACM-CpG) induces a robust neutralizing antibody response as well as functional memory $CD4^+$ and $CD8^+$ T cells that persist at least 40 days after the last administration. The efficient targeting of both DC1 and DC2 by ACM polymersomes ensures that antigen and adjuvant payloads are delivered to both cell types for the induction of a multifaceted adaptive immune response. Inclusion of CpG in the vaccine formulation confers several benefits. It potently activates DCs to upregulate co-stimulatory molecules, including CD40, CD80, and CD86,[55] which promotes T cell activation and B cell antibody class switch and secretion.[56,57] Binding of CpG to TLR9 triggers mitogen-activated protein kinase (MAPK) and nuclear factor kappa B (NF-κB) signaling that results in pro-inflammatory cytokine production and a Th1-skewed immune response.[58,59] In our study, such polarization is clearly demonstrated by the cytokine profile of $CD4^+$ T cells of the CpG-containing vaccine formulations. In the absence of CpG, we consistently observed IL-5 production, which fits a broader picture of an inherent Th2 skew from immunizing with protein antigens of viral and nonviral origins.[60,61] From a safety standpoint, this represents a potential risk of Th2 immunopathology, best exemplified by whole-inactivated respiratory syncytial virus (RSV) vaccines.[34,62] Accordingly, such vaccines primed the immune system for a Th2-biased response during actual infection, and the resultant production of Th2 cytokines promoted increased mucus production, eosinophil recruitment, and airway hyperreactivity. Therefore, skewing of the immune response to Th1 by CpG is likely to improve vaccine safety.

We have shown that neutralizing titers can remain stable despite rapidly declining total IgG, which resembles SARS-CoV-2-infection in humans.[63] This may be due to affinity maturation, which progressively selects for high avidity, strongly neutralizing antibodies while excluding weaker binders. Additionally, compared to the neutralizing titers measured in convalescent patients recruited in Singapore,[64] it appears that our vaccine formulation may be more efficient in triggering neutralizing antibodies. Neutralizing antibodies are highly predictive of protection from symptomatic SARS-CoV-2 infection[65] and could potentially serve as a correlate of protection. Reports of asymptomatic or mild patients producing widely varying neutralizing antibody levels, including a minority with no detectable neutralizing response,[4,66] underscore the unpredictability of a natural infection. In this regard, our vaccine can perhaps facilitate the induction of a more uniform neutralizing antibody response.

The role of T cells in SARS-CoV-2 is arguably less clear than antibodies. Nevertheless, several studies have confirmed the induction of a T cell response following infection. Early in the adaptive immune response against SARS-CoV-2, T cells are robustly activated.[31] Patients who recovered from SARS in 2003 possessed memory T cells that could be detected 17 years after.[64] Additionally, individuals with no history of SARS, Covid-19, or contact with individuals who had SARS and/or Covid-19 possessed cross-reactive T cells that may be generated by a previous infection with other betacoronaviruses.[64] These data suggested that the SARS-CoV-2-specific T cell response may be similarly durable. In a study examining the T cell specificities of Covid-19 convalescent patients, spike-specific $CD4^+$ T cells were consistently detected, whereas $CD8^+$ T cells were present in most subjects.[10] This implies that a spike-based vaccine may generate a cellular immune response that largely recapitulates the $CD4^+$ T cell profile of a natural infection, albeit with a narrower $CD8^+$ T cell repertoire.

One major challenge in creating a pandemic vaccine is generating sufficient doses of high-quality antigen to rapidly meet global demand. As such, dose-sparing strategies are critical, and this has traditionally been achieved using adjuvants. On the basis of our work, we believe that ACM technology can further augment the dose-sparing effect. We have shown this approach to greatly improve vaccine immunogenicity, such that even the 1/10th dose retains a substantial level of efficacy. While further titration experiments are required to determine the optimum dose, the present limited investigation strongly supports the use of ACM technology to address limited antigen availability in a pandemic.

Another challenge concerns the rapid emergence of new variants of concern exhibiting enhanced transmissibility and/or antibody escape, which would necessitate periodic boosters with new spike proteins. In this regard, having a nonimmunogenic carrier, such as ACM polymersomes, is advantageous to avoid the induction of antivector responses that can potentially attenuate the viral-specific immune response.[67] Apart from this, our modular approach of combining ACM-S1S2 with ACM-CpG allows us to easily replace existing spike protein with those of new variants for a more rapid response. Moreover, manufacturing is also simplified by this strategy, given the difficulty of controlling the quantity of both materials being encapsulated within the same polymersome. Finally, from the perspective of the immune response, we have shown that coadministering ACM-CpG with ACM-S1S2 confers significant improvement in the antibody and T cell responses. This indicates that coencapsulation of antigen and adjuvant within the same vesicle is not strictly required to achieve the enhancement of the antigen-specific response, a finding that is in line with a recent study demonstrating effective vaccination with co-delivery of antigen and CpG adjuvant in separate virus-like particles (VLPs).[68]

MATERIALS AND METHODS

Materials. Murine CpG 1826 (T*C*C*A*T*-G*A*C*G*T*T*C*C*T*G*A*C*G*T*T, where * denotes phosphorothioate backbone) was purchased from InvivoGen. Rhodamine B-terminated PEG_{13}-*b*-PBD_{22} was purchased from Polymer Source Inc. DQ-OVA was purchased from Life Technologies, Thermo Fisher

https://doi.org/10.1021/acsnano.1c01243
ACS Nano 2021, 15, 15754−15770

Scientific. DOTAP was from Avanti Polar Lipids. Triton-X 100 was from MP Biomedicals. All other chemicals were purchased from Sigma-Aldrich unless stated otherwise. The trimeric spike protein was purchased from ACROBiosystems, and the S2 domain protein from Sino Biological.

Protein Expression. Recombinant SARS-CoV-2 spike protein containing only the ectodomain (hereby referred to as "S1S2"), from Genbank entry MN908947.3, with a mutated furin cleavage site (NSPRRAR → NSNQSAR) and a melittin secretion leader, was expressed *via* T.ni insect cells (Hi5, Thermo Fisher Scientific). The gene of interest was placed into the Bac-to-Bac system (Thermo Fisher Scientific), transfected, and passaged in Sf9 cells (Thermo Fisher Scientific) until a high titer was achieved. T.ni cells, diluted to 1.5×10^6 cells/mL, were infected at a MOI of 0.1 and left to incubate (27 °C for 96 h, shaking at 125 rpm). The cell culture was harvested, and the cells were removed by centrifugation (3500*g* for 15 min at 4 °C) and clarified by 0.22 μm filtration. The media containing the protein of interest was first concentrated to a tenth of the original volume *via* Tangential flow filtration hollow fiber cassettes (10 kDa hollow fiber cassette; Cytiva), followed by 5 volumes worth of diafiltration into IEX binding buffer (20 mM phosphate, 50 mM NaCl, 5% sucrose, 5% glycerol, 0.025% Tween 20, 1 mM EDTA, pH 4.6). The protein was initially purified by first binding the sample in a HiTrap FF SP column (5 mL; Cytiva) using a GE AKTA system loaded with Unicorn software, set at 2 mL/min. Once the sample had been loaded and washed with 5 column volumes of IEX binding buffer, the protein of interest was eluted off the column by switching to IEX elution buffer (20 mM phosphate, 50 mM NaCl, 5% sucrose, 5% glycerol, 0.025% Tween 20, 1 mM EDTA, pH 7.6). The eluted sample was concentrated using a Vivaspin concentrator (10 kDa, 15 mL, PES; Sartorius) to a 5 mL volume. The protein was polished by loading 2.5 mL of sample in a 5 mL loading loop onto a Hiload 16/60 Superdex 200 Prep grade column, running with SEC buffer (20 mM phosphate, 150 mM NaCl, 5% sucrose, pH 7.6) at 1 mL/min. Purified protein was analyzed for size by injection of 100 μL of sample into a Superdex 200 increase 10/300 GL column using a GE AKTA system running at 0.75 mL/min. Molecular mass of the protein was calculated *via* comparison with an HMW gel filtration calibration kit (containing a mixture of thyroglobulin, ferritin, aldose and conalbumin; Cytiva).

Preparation of ACM-Antigen Polymersomes. ACM polymersomes encapsulating spike trimer, S1S2, and S2 proteins were prepared by the solvent dispersion method, followed by extrusion. A 400 mg/mL stock solution of DOTAP and PEG_{13}-*b*-PBD_{22} polymer was prepared by dissolving solid DOTAP and polymer in tetrahydrofuran (THF, Tedia HPLC grade, cat. no. TS2121). A 0.15 equiv (1.5 μmol) amount of DOTAP stock solution and 0.85 equiv (8.5 μmol) of polymer stock solution were mixed in a 2 mL glass vial (Agilent, cat. no. 8010-0542) and vortexed for 30 s to prepare solution A. After mixing, a defined amount of solution A was aspirated in a 50 μL Hamilton glass syringe. A 1 mL solution of 100 μg/mL antigen was placed in a 5 mL glass test tube (solution B). Solution A was added slowly (with the addition rate of roughly 2 mL/h) to 1 mL of solution B while constantly mixing (600–700 rpm) at room temperature. A turbid solution was obtained. The resultant solution was extruded 21 times through a 200 nm Nuclepore hydrophilic polycarbonate membrane filter using a 1 mL mini-extruder (Avanti Polar Lipids, cat. no. 610000) to get monodispersed ACM-antigen vesicles. Nonencapsulated antigens were removed by overnight dialysis. Encapsulation of antigen was quantified by densiometric analysis using a known BSA standard in Fiji ImageJ software (v. 1.52a).

Preparation of ACM-CpG Polymersomes. ACM-CpG polymersomes were prepared by the solvent dispersion method above, followed by extrusion. A 50 μL amount of the 400 mg/mL stock solution containing DOTAP and PEG13-*b*-PBD22 polymer was added dropwise (with the addition rate of roughly 2 mL/h) to 1 mL of CpG solution. A turbid solution was obtained. The resultant solution was extruded 21 times through a 200 nm Nuclepore hydrophilic polycarbonate membrane filter using a 1 mL mini-extruder to get monodispersed ACM-CpG polymersomes. Unencapsulated CpG was removed by overnight dialysis using 300 kDa molecular weight cutoff (MWCO) cellulose ester membrane (Spectrum Laboratories Inc., cat. no. 131450) against PBS, pH 7.4 at 4 °C.

Preparation of ACM-Rhodamine and ACM-Rhodamine/DQ-OVA. ACM-Rhodamine and ACM-Rhodamine/DQ-OVA were prepared by the thin-film rehydration method, followed by extrusion. A 9.9 mg amount of PEG_{13}-*b*-PBD_{22} polymer in chloroform was mixed with 0.1 mg of Rhodamine B-terminated PEG_{13}-*b*-PBD_{22} in chloroform with a ratio of 99:1 w/v shaken in a 10 mL round-bottom flask. After mixing, chloroform was removed by rotary evaporator followed by drying for 1 h at high vacuum. A 1 mL solution of 100 μg/mL DQ-OVA was placed in the flask with a Teflon-coated magnetic stirrer bar for the preparation of ACM-Rhodamine/DQ-OVA; for ACM-Rhodamine, 1 mL of buffer was added. The solution was stirred at 600–700 rpm with aluminum foil covered overnight at 4 °C. A pink-colored turbid solution was obtained. The resultant solution was extruded 21 times through a 200 nm Nuclepore hydrophilic polycarbonate membrane filter using a 1 mL mini-extruder (Avanti Polar Lipids, cat. no. 610000) to get monodispersed ACM nanoparticles. Nonencapsulated DQ-OVA was removed by overnight dialysis using a 300 kDa MWCO cellulose ester membrane (Spectrum Laboratories Inc., cat. no. 131450) against 1× PBS at 4 °C.

Particle Size Measurement by Dynamic Light Scattering. DLS was performed on the Zetasizer Nano ZS system (Malvern Panalytical). A 100 μL amount of the 20-fold-diluted, purified, filtered sample was placed in a microcuvette (Eppendorf UVette; Sigma-Aldrich), and an average of 30 runs (10 s per run) were collected using the 173° detector.

Quantification of Spike Protein by SDS-PAGE. A 20 μL amount of ACM-spike protein or free spike protein at known concentrations was added to microcentrifuge tubes. A 2 μL amount of 25% Triton-X 100 was added to each sample and incubated for 30 min at 25 °C to lyse ACM vesicles. Next, 20 μL of 1× gel loading dye buffer was added, and the tubes were shaken at 95 °C for 10 min. A 20 μL amount of each sample was migrated on 4–12% Bis-Tris SDS-PAGE gel at 140 V for 40 min. The completed gel was fixed and then stained with SYPRO Ruby protein gel stain (Molecular Probes, Thermo Fisher Scientific).

Western Blot. Proteins were transferred from SDS-PAGE gel to PVDF membrane using the iBlot 2 dry blotting system (Thermo Fisher Scientific). The membrane was blocked 1 h at room temperature with 5% w/v nonfat milk dissolved in TBST (Tris-buffered saline with 0.1% v/v Tween-20). Mouse serum raised against a recombinant SARS-CoV-2 spike protein (purchased from Sino Biological) was diluted 1:6000 and incubated with the membrane for 1 h at room temperature. The membrane was washed thrice with TBST for a total of 30 min before incubating 1 h at room temperature with HRP-conjugated goat anti-mouse secondary antibody at a 1:10 000 dilution. After three final washes with TBST, the membrane was briefly incubated with ECL substrate (Pierce, Thermo Fisher Scientific). Chemiluminescent signals were captured using the ImageQuant LAS 500 system (Cytiva).

Quantification of CpG by Fluorescence. A 20 μL portion of ACM-CpG or free CpG at known concentrations was added to a 384-well black plate. A 20 μL amount of PBS with 10% Triton-X 100 was added into each well, and the plate was incubated for 30 min at 25 °C to lyse ACM vesicles before adding 10 μL of 20× SYBR Safe DNA gel stain (Invitrogen, Thermo Fisher Scientific). The plate was incubated for 5 min at 25 °C, and fluorescence was measured (excitation, 500 nm; emission, 530 nm) using a plate reader (Biotek).

Cryogenic-Transmission Electron Microscopy. For cryo-TEM, 4 μL of the samples containing ACM-S1S2, ACM-CpG, and ACM-S1S2 + ACM-CpG vesicles (5 mg/mL) was adsorbed onto a lacey holey carbon-coated Cu grid, 200 mesh size (Electron Microscopy Sciences). The grid was surface treated for 20 s *via* glow discharge before use. After surface treatment, a 4 μL sample was added and the grid was blotted with Whatman filter paper (GE Healthcare Bio-Sciences) for 2 s with blot force 1 and then plunged into liquid ethane at −178 °C using a Vitrobot (FEI Company). The cryo-grids were imaged using a FEG 200 keV transmission electron microscope (Arctica; FEI Company) equipped with a direct electron detector (Falcon II; Fei Company). Images were analyzed in Fiji ImageJ software (v. 1.52a), and membrane thickness of vesicles was calculated by counting at least 20 particles.

MTT Assay. HEK293T cells were routinely cultured in RPMI-1640 medium supplemented with 10% v/v heat-inactivated fetal bovine

https://doi.org/10.1021/acsnano.1c01243
ACS Nano 2021, 15, 15754–15770

serum (FBS) and 1× penicillin/streptomycin. Cell culture media and reagents were purchased from Thermo Fisher Scientific. To perform the MTT assay, HEK293T cells were seeded in a 96-well U-bottom plate at a density of 4×10^5/mL in 100 μL per well and incubated 24 h at 37 °C, 5% CO_2. Cells were subsequently washed once with fresh medium, and ACM formulations were applied in triplicates at 100 μL per well. Cells were incubated for 24 h before MTT reagent (Sigma-Aldrich) was added at 0.5 mg/mL. After 4 h of incubation, 100 μL of Solubilization Solution was added per well, and the plate was allowed to stand overnight in the incubator for complete solubilization of purple formazan crystals. Absorbance was measured at 550 nm with wavelength correction at 690 nm.

Mice (Investigation of DC Targeting by ACM Polymersomes). C57BL/6 mice were purchased from InVivos. All mice were maintained in the Singapore Immunology Network (SIgN) animal facility before use at 7−10 weeks of age. All experiments and procedures were approved by the Institutional Animal Care and Use Committee of the Biological Resource Center (Agency for Science, Technology and Research, Singapore) in accordance with the guidelines of the Agri-Food and Veterinary Authority and the National Advisory Committee for Laboratory Animal Research of Singapore (ICUAC No. 181357). To investigate *in vivo* ACM-CpG release, mice were SC injected with empty ACM or 5 μg of free CpG or ACM-CpG. Draining LNs (inguinal) were harvested 2 days later for the assessment of DC activation by flow cytometry.

Mice (Vaccination). This study was performed at the Biological Resource Center (Agency for Science, Technology and Research, Singapore). Female C57BL/6 mice were purchased from InVivos and used at 8−9 weeks of age. Seven to eight mice were assigned to each vaccine formulation, unless stated otherwise. Mice were administered 5 μg of a respective antigen (free or encapsulated) with or without 5 μg of CpG adjuvant (free or encapsulated) in a 200 μL volume per dose *via* the SC route, for one prime and one boost separated by 14 days. Blood was collected on days 13, 28, 40, and 54; spleens were collected on the final time point of day 54. This study was done in accordance with approved IACUC protocol 181137.

Mouse Tissue Preparation and Data Analysis for Flow Cytometry. Mice were injected SC with 100 μL of PBS, 100 μL of ACM-Rhodamine, or 100 μL of ACM-Rhodamine/DQ-OVA and analyzed on day 1, 3, or 6 postinjection. Back skin from the injection site was harvested and placed in RPMI1640 (Gibco, Thermo Fisher Scientific) containing Dispase for 90 min at 37 °C. The back skin and skin-draining LNs (separately) then were transferred into RPMI1640 containing deoxyribonuclease I (Roche) and collagenase (Sigma-Aldrich), disrupted using scissors or tweezers, and digested for 30 min at 37 °C. Digest was stopped by adding PBS + 10 mM EDTA, and cell suspensions were transferred into a fresh tube over a 70 μm nylon mesh sieve. If necessary, red blood cells were lysed using RBC lysis buffer (eBioscience), and single-cell suspensions were passed through a 70 μm nylon mesh sieve before further use. Single-cell suspensions then were stained for flow cytometry analysis following standard protocols. Monoclonal antibodies against Ly6C (clone HK1.4), CD11b (clone M1/70), EpCAM (clone G8.8), CD64 (clone X54-5/7.1), and F4/80 (clone BM8) were purchased from BioLegend, CD11c (clone N418), CD103 (clone 2E7), CD8a (clone 53-6.7), and MHC-II (clone M5/114.15.2) were purchased from eBioscience, CD24 (clone M1/69), CD3 (clone 500A2), CD45 (clone 30-F11), CD49b (clone HMa2), and Ly6G (clone 1A8) were purchased from BD Bioscience, and CD19 (clone 1D3) and Streptavidin for conjugation of biotinylated antibodies were purchased from BD Horizon. DAPI staining was used to allow identification of cell doublets and dead cells. Flow cytometry acquisition was performed on a five-laser LSR II (BD) using FACSDiva software, and data were subsequently analyzed with FlowJo v.10.5.3 (Tree Star).

Intracellular Cytokine Staining. Single-cell suspensions of splenocytes were generated by pushing each spleen through a 70 μm cell strainer. Red blood cells were lysed using 1× RBC lysis buffer (eBioscience, Thermo Fisher Scientific) for 5 min at room temperature. Splenocytes were resuspended in complete cell culture medium (RPMI 1640 supplemented with 10% v/v heat-inactivated FBS, 50 μM β-mercaptoethanol, 2 mM L-glutamax, 10 mM HEPES, and 100 U/ml pen/strep; all materials purchased from Gibco, Thermo Fisher Scientific) and seeded in a 96-well U-bottom plate at a density of ∼3 million per well. Splenocytes were incubated with an overlapping peptide pool covering the spike protein (JPT product PM-WCPV-S-1 vials 1 and 2) along with functional anti-mouse CD28 and CD49d antibodies overnight at 37 °C, 5% CO_2. Peptides and antibodies were used at 1 μg/mL, respectively. Negative control wells were generated by incubating splenocytes with culture medium and costimulatory antibodies. Positive control wells were generated by incubating splenocytes with 20 ng/mL PMA (Sigma-Aldrich) and 1 μg/mL ionomycin (Sigma-Aldrich). The following morning, cytokine secretion was blocked with 1× brefeldin A (eBioscience) and 1× monensin (eBioscience) for 6 h. Subsequently, cells were stained with fixable viability dye eFluor 455UV (eBioscience) at 1:1000 in PBS for 30 min at 4 °C. Cells were washed with FACS buffer (1× PBS supplemented with 2% v/v heat-inactivated FBS and 1 mM EDTA) and stained for surface markers with the following antibodies purchased from BioLegend, eBioscience, and BD: BUV395-CD45 (30-F11), Brilliant Violet 785-CD3 (17A2), Alexa Fluor 700-CD4 (GK1.5), APC-eFluor 780-CD8 (53-6.7), and PE/Dazzle 594-CD44 (IM7). Antibodies were diluted 1:200 with FACS buffer and incubated with cells for 30 min at 4 °C. Fixation and permeabilization were done using the Cytofix/Cytoperm kit (BD), according to the manufacturer's instructions. Intracellular cytokines were stained with the following antibodies: Alexa Fluor 488-IFNγ (XMG1.2), Brilliant Violet 650-TNFα (MP6-XT22), APC-IL-2 (JES6-5H4), PerCP-eFluor 710-IL-4 (11B11), and PE-IL-5 (TRFK5). Antibodies were diluted 1:200 with 1× permeabilization buffer and incubated with cells for 30 min at 4 °C. Cells were washed with 1× permeabilization buffer and then resuspended in FACS buffer for analysis with the LSR II flow cytometer (BD). Approximately 600 00 total events were recorded for each sample. Data analysis was performed using FlowJo V10.6.2 software. Percentages of cytokine-positive events for immunized mouse groups were compared against the PBS-control group. Responses above the background of the PBS-control group were considered spike-specific.

ACM Uptake in Human PBMC. Blood samples were obtained from healthy donors after providing written informed consent to participate in research protocols approved by the Institutional Review Board of SIgN. PBMCs were isolated by Ficoll-Paque (GE Healthcare) density gradient centrifugation of apheresis. Isolated PBMCs were cultured overnight in RPMI1640 medium supplemented with 2% human AB serum and 1% penicillin/streptomycin (Gibco, Thermo Fisher Scientific) in 96-well round-bottom tissue plates, at 37 °C, with or without ACM-Rhodamine (1:50 or 1:250 dilution). PBMCs then were stained for flow cytometry following standard protocols; briefly, 5×10^6 cells/tube were washed and incubated with live/dead blue dye (Invitrogen) for 30 min at 4 °C in PBS, followed by incubation in 5% heat-inactivated FCS for 15 min at 4 °C (Sigma-Aldrich). Antibodies were diluted in PBS with 2% FCS and 2 mM EDTA, added to the cells, and incubated for 30 min at 4 °C. PBMCs were stained with mouse anti-human monoclonal surface antibodies (mAbs) against CD45 (clone HI30), CD3 (clone SP34-2), CD19 (clone SJ25C1), CD20 (clone 2H7), CD14 (clone M5E2), and CD123 (clone 7G3) purchased from BD Biosciences, mAbs against HLA-DR (clone L243), CD16 (clone 3G8), and CD1c (clone L161) purchased from BioLegend, and mAb against CD141 (clone AD5-14H12) purchased from Miltenyi. Flow cytometry was performed on a BD FACSFortessa (BD Biosciences). Data were analyzed using FlowJo v.10.5.3 (Tree Star).

ACE2-Binding Assay. Spike protein was coated onto 96-well EIA/RIA high binding plates (Corning) in carbonate-bicarbonate buffer (15 mmol/L Na_2CO_3, 35 mmol/L $NaHCO_3$; pH 9.6) at 200 ng per well, overnight at 4 °C. Plates were blocked with 2% BSA in TBS + 0.05% v/v Tween-20 for 1.5 h at 37 °C. Threefold serial dilutions of recombinant hACE2-Fc protein (12 000 ng/mL to 0.61 ng/mL; GenScript) were prepared in TBS buffer containing 0.5% w/v BSA and applied to the plate for 1 h at 37 °C. HRP-conjugated goat anti-human IgG (Fc specific; Sigma-Aldrich) was diluted 1:10 000 and applied to the plate for 1 h at 37 °C. ACE2-binding was visualized by addition of TMB substrate (Sigma-Aldrich) for 15 min at room temperature, and the

https://doi.org/10.1021/acsnano.1c01243
ACS Nano 2021, 15, 15754−15770

reaction was terminated with Stop Solution (Invitrogen, Thermo Fisher Scientific). Absorbance was measured at 450 nm using a microplate reader (Biotek). Background absorbance was subtracted and the EC_{50} value of the titration curve was determined using GraphPad Prism version 8.4.3 with five-parameter nonlinear regression.

SARS-CoV-2 Spike-Specific Serum IgG. Homemade spike protein was coated onto a 96-well EIA/RIA high binding plate (Corning) at 100 ng per well in PBS overnight at 4 °C. Plates were blocked with 2% w/v BSA in PBS + 0.1% v/v Tween-20 for 1.5 h at 37 °C. Mouse sera were serially diluted from an initial 1:100 with blocking buffer and applied to the plate for 1 h at 37 °C. HRP-conjugated goat anti-mouse IgG (H/L) (BioRad) was diluted in blocking buffer at 1:10 000 and applied to the plate for 1 h at 37 °C. Antibody binding was visualized by addition of TMB substrate for 10 min at room temperature, and the reaction was terminated with Stop Solution. Absorbance was measured at 450 nm. Each titration curve was analyzed *via* five-parameter nonlinear regression (GraphPad Prism V8.4.3) to calculate end point titer, which was defined as the highest dilution producing an absorbance three times the plate background.

Serum Neutralizing Antibody by Competitive ELISA. The cPass SARS-CoV-2 Surrogate virus neutralization test kit (GenScript) was used according to the manufacturer's instructions. Briefly, each serum sample was diluted 1:10 using sample dilution buffer and incubated with an equal volume of HRP-RBD solution for 30 min at 37 °C. The mix was then applied to eight-well strips precoated with ACE2 protein for 15 min at 37 °C. RBD-ACE2 binding was visualized by addition of TMB substrate for 15 min at room temperature. Reaction was terminated using Stop Solution, and absorbance was measured at 450 nm. Inhibition of RBD-ACE2 binding was calculated using the formula:

$$\left(1 - \frac{OD_{\text{value of sample}}}{OD_{\text{value of negative control}}}\right) \times 100\%$$

Pseudovirus Neutralization Test. Pseudotyped lentiviral particles harboring the SARS-CoV-2 spike glycoprotein (S-pp) were generated by co-transfection of 293FT cells with S expression plasmid and envelope-defective pNL4-3.Luc.R-E- luciferase reporter vector. The S expression plasmid was constructed by cloning the codon-optimized spike gene (according to GenBank accession QHD43416.1) containing a 19 amino acid C-terminal truncation to enhance pseudotyping efficiency[51] into the pTT5 mammalian expression vector (pTT5LnX-coV-SP, a kind gift from Brendon John Hanson, Biological Defense Program, DSO National Laboratories, Singapore). The viral supernatant was collected 48−72 h post-transfection, clarified by centrifugation, and stored at −80 °C until use. S-pp titer was determined using a lentivirus-associated p24 ELISA kit (Cell Biolabs, Inc., San Diego, CA, USA). CHO cells stably overexpressing human ACE2 (CHO-ACE2)[69] were seeded in 96-well plates 24 h before transduction. Mouse serum samples were diluted 1:20 in culture medium, inactivated at 56 °C for 30 min, and sterilized using Ultrafree-MC centrifugal filters (Millipore, Burlington, MA, USA). For S-pp neutralization assays, the serum samples were 2-fold serially diluted six times and incubated with S-pp for 1 h at room temperature before the mixture was added to target cells in triplicate wells. Cells were incubated at 37 °C for 48 h before being tested for luciferase activity using the Bright-Glo luciferase assay system (Promega, Madison, WI, USA). Luminescence was measured using a plate reader (Tecan Infinite M200), and after subtraction of background luminescence, the data were expressed as a percentage of the reading obtained in the absence of serum (cells + S-pp only), which was set at 100%. Dose−response curves were plotted with a four-parameter nonlinear regression using GraphPad Prism 8, and neutralizing titers were reported as the serum dilution that blocked 50% S-pp entry (IC_{50}). Samples that did not achieve 50% neutralization at the input serum dilution (1:40) were expressed as 1, while the neutralizing titer of samples that achieved more than 50% neutralization at the highest serum dilution (1:1280) was reported as 1280.

SARS-CoV-2 Neutralization Test. Serum samples were serially diluted 2-fold in DMEM supplemented with 5% v/v FBS, from an initial of 1:10, and incubated with an equal volume of viral suspension (1×10^4 $TCID_{50}$/mL) for 90 min at 37 °C. The mixture was transferred to Vero-E6 cells and incubated for 1 h at 37 °C. The inoculum was removed, and cells were washed once with DMEM. Fresh culture medium was added, and cells were incubated for 4 days at 37 °C. The assay was performed in duplicate. Neutralization titer was defined as the highest serum dilution that fully inhibited a cytopathic effect.

Statistics. Statistical analyses were performed using GraphPad Prism software (version 9.2.0). For comparison of antibody titers between treatment groups across multiple time points or activation markers on DC subsets between treatment groups, two-way ANOVA with Tukey's or Sidak's multiple comparison was used, where appropriate. For comparison of antibody titers or T cell responses between treatment groups at a single time point, one-way ANOVA with Tukey's multiple comparison was used. Significant differences are indicated where present. *: $P \leq 0.05$; **: $P \leq 0.01$; ***: $P \leq 0.001$; ****: $P \leq 0.0001$; ns: not significant.

ASSOCIATED CONTENT

Supporting Information

The Supporting Information is available free of charge at https://pubs.acs.org/doi/10.1021/acsnano.1c01243.

Characterization of S1S2 by size exclusion chromatography, endotoxin measurements of ACM formulations, protein concentration measurements, stability studies, human PBMC uptake study, murine DC uptake study, Pearson correlation between pseudovirus and live virus neutralization tests, and cytokine profiles of memory T cells from immunized mice (PDF)

AUTHOR INFORMATION

Corresponding Author

Madhavan Nallani − *ACM Biolabs Pte Ltd, Singapore 638075, Singapore*; Phone: +65 62655646; Email: mnallani@acmbiolabs.com

Authors

Jian Hang Lam − *ACM Biolabs Pte Ltd, Singapore 638075, Singapore*; orcid.org/0000-0003-3378-350X

Amit K. Khan − *ACM Biolabs Pte Ltd, Singapore 638075, Singapore*

Thomas A. Cornell − *ACM Biolabs Pte Ltd, Singapore 638075, Singapore*

Teck Wan Chia − *ACM Biolabs Pte Ltd, Singapore 638075, Singapore*

Regine J. Dress − *Agency for Science, Technology and Research, Singapore 138648, Singapore*

Wen Wang William Yeow − *ACM Biolabs Pte Ltd, Singapore 638075, Singapore*

Nur Khairiah Mohd-Ismail − *Infectious Diseases Translational Research Program, Department of Microbiology and Immunology, Yong Loo Lin School of Medicine, National University Health System, National University of Singapore, Singapore 117545, Singapore*

Shrinivas Venkataraman − *ACM Biolabs Pte Ltd, Singapore 638075, Singapore*

Kim Tien Ng − *Infectious Diseases Translational Research Program, Department of Microbiology and Immunology, Yong Loo Lin School of Medicine, National University Health System, National University of Singapore, Singapore 117545, Singapore*

Yee-Joo Tan − *Infectious Diseases Translational Research Program, Department of Microbiology and Immunology, Yong Loo Lin School of Medicine, National University Health*

System, National University of Singapore, Singapore 117545, Singapore; Institute of Molecular and Cell Biology, Agency for Science, Technology and Research, Singapore 138673, Singapore

Danielle E. Anderson − *Program in Emerging Infectious Diseases, Duke-NUS Medical School, Singapore 169857, Singapore*

Florent Ginhoux − *Agency for Science, Technology and Research, Singapore 138648, Singapore; SingHealth Translational Immunology and Inflammation Centre, Singapore 169856, Singapore*

Complete contact information is available at: https://pubs.acs.org/10.1021/acsnano.1c01243

Author Contributions

The manuscript was written through contributions of all authors. J.H.L., A.K.K., T.A.C., R.J.D., T.W.C., W.W.W.Y., N.K.M.I., K.T.N., and D.E.A. designed and performed the experiments. Y.J.T., R.J.D., F.G., and M.N. designed the experiments, analyzed the data, and provided critical intellectual input. J.H.L., A.K.K., S.V., R.J.D., and M.N. wrote the manuscript. All authors have given approval to the final version of the manuscript.

Funding

We would like to acknowledge IAF-ICP, A*STAR grant for ACM-SIgN collaboration and NHIC Gap Funding Award (NHIC-COV19-2005008) for collaboration with Dr. Francesca Lim, Singapore General Hospital, and Dr. Danielle E. Anderson, Duke-NUS Medical School, Singapore. The work performed in NUS/NUHS was supported by NUHS Research Office under Project Number NUHSRO/2020/033/RO5+5/CORONAVIRUS/LOA (WBS R-571-000-071-733).

Notes

The authors declare the following competing financial interest(s): D.E.A. developed the cPass kit; J.H.L, A.K.K., T.A.C., T.W.C., W.W.W.Y., S.V., and M.N. are employees of ACM Biolabs Pte Ltd; F.G. is part of the ACM SAB.

A preprint version of this work is available online: Jian Hang Lam; Amit Kumar Khan; Thomas Andrew Cornell; Regine Josefine Dress; Teck Wan Chia; Wen Wang William Yeow; Nur Khairiah Mohd-Ismail; Shrinivas Venkataraman; Kim Tien Ng; Yee-Joo Tan; Danielle E. Anderson; Florent Ginhoux; Madhavan Nallani. Next Generation Vaccine Platform: Polymersomes as Stable Nanocarriers for a Highly Immunogenic and Durable SARS-CoV-2 Spike Protein Subunit Vaccine. 2021.01.24.427729. bioRxiv. https://doi.org/10.1101/2021.01.24.427729 (accessed Sept 25, 2021).

ACKNOWLEDGMENTS

We would like to thank Aw Ting Yan (ACM Biolabs), Nicholas Chng Jianyao (ACM Biolabs), and Liam Thomas Martin (ACM Biolabs) for assisting in protein expression in insect cells and optimization of protein purification; James Ho (CBSS, NTU) for helping with Cryo EM sample preparation, and Andrew Wong (NTU) for Cryo EM sample measuring; and Joey Poh Soh Yee and the staff of BRC (A*STAR) for assisting in mouse immunization and sample collection.

REFERENCES

(1) Zhang, R.; Li, Y.; Zhang, A. L.; Wang, Y.; Molina, M. J. Identifying Airborne Transmission as the Dominant Route for the Spread of COVID-19. *Proc. Natl. Acad. Sci. U. S. A.* **2020**, *117* (26), 14857−14863.

(2) Sia, S. F.; Yan, L.-M.; Chin, A. W. H.; Fung, K.; Choy, K.-T.; Wong, A. Y. L.; Kaewpreedee, P.; Perera, R. A. P. M.; Poon, L. L. M.; Nicholls, J. M.; Peiris, M.; Yen, H.-L. Pathogenesis and Transmission of SARS-CoV-2 in Golden Hamsters. *Nature* **2020**, *583* (7818), 834−838.

(3) Richard, M.; Kok, A.; de Meulder, D.; Bestebroer, T. M.; Lamers, M. M.; Okba, N. M. A.; Fentener van Vlissingen, M.; Rockx, B.; Haagmans, B. L.; Koopmans, M. P. G.; Fouchier, R. A. M.; Herfst, S. SARS-CoV-2 Is Transmitted *via* Contact and *via* the Air between Ferrets. *Nat. Commun.* **2020**, *11* (1), 3496.

(4) Wu, Z.; McGoogan, J. M. Characteristics of and Important Lessons from the Coronavirus Disease 2019 (COVID-19) Outbreak in China: Summary of a Report of 72 314 Cases from the Chinese Center for Disease Control and Prevention. *JAMA* **2020**, *323* (13), 1239−1242.

(5) Gorbalenya, A. E.; Baker, S. C.; Baric, R. S.; de Groot, R. J.; Drosten, C.; Gulyaeva, A. A.; Haagmans, B. L.; Lauber, C.; Leontovich, A. M.; Neuman, B. W.; Penzar, D.; Perlman, S.; Poon, L. L. M.; Samborskiy, D. V.; Sidorov, I. A.; Sola, I.; Ziebuhr, J. Coronaviridae Study Group of the International Committee on Taxonomy of, V., the Species Severe Acute Respiratory Syndrome-Related Coronavirus: Classifying 2019-nCoV and Naming It SARS-CoV-2. *Nature Microbiology* **2020**, *5* (4), 536−544.

(6) Ke, Z.; Oton, J.; Qu, K.; Cortese, M.; Zila, V.; McKeane, L.; Nakane, T.; Zivanov, J.; Neufeldt, C. J.; Cerikan, B.; Lu, J. M.; Peukes, J.; Xiong, X.; Kräusslich, H.-G.; Scheres, S. H. W.; Bartenschlager, R.; Briggs, J. A. G., Structures and Distributions of SARS-CoV-2 Spike Proteins on Intact Virions. *Nature* **2020**, *588*, 498502.

(7) Walls, A. C.; Park, Y.-J.; Tortorici, M. A.; Wall, A.; McGuire, A. T.; Veesler, D. Structure, Function, and Antigenicity of the SARS-CoV-2 Spike Glycoprotein. *Cell* **2020**, *181* (2), 281−292.

(8) Chi, X.; Yan, R.; Zhang, J.; Zhang, G.; Zhang, Y.; Hao, M.; Zhang, Z.; Fan, P.; Dong, Y.; Yang, Y.; Chen, Z.; Guo, Y.; Zhang, J.; Li, Y.; Song, X.; Chen, Y.; Xia, L.; Fu, L.; Hou, L.; Xu, J.; Yu, C.; Li, J.; Zhou, Q.; Chen, W. A Neutralizing Human Antibody Binds to the N-Terminal Domain of the Spike Protein of SARS-CoV-2. *Science* **2020**, *369* (6504), 650−655.

(9) Rogers, T. F.; Zhao, F.; Huang, D.; Beutler, N.; Burns, A.; He, W.-t.; Limbo, O.; Smith, C.; Song, G.; Woehl, J.; Yang, L.; Abbott, R. K.; Callaghan, S.; Garcia, E.; Hurtado, J.; Parren, M.; Peng, L.; Ramirez, S.; Ricketts, J.; Ricciardi, M. J.; Rawlings, S. A.; Wu, N. C.; Yuan, M.; Smith, D. M.; Nemazee, D.; Teijaro, J. R.; Voss, J. E.; Wilson, I. A.; Andrabi, R.; Briney, B.; Landais, E.; Sok, D.; Jardine, J. G.; Burton, D. R. Isolation of Potent SARS-CoV-2 Neutralizing Antibodies and Protection from Disease in a Small Animal Model. *Science* **2020**, *369* (6506), 956−963.

(10) Grifoni, A.; Weiskopf, D.; Ramirez, S. I.; Mateus, J.; Dan, J. M.; Moderbacher, C. R.; Rawlings, S. A.; Sutherland, A.; Premkumar, L.; Jadi, R. S.; Marrama, D.; de Silva, A. M.; Frazier, A.; Carlin, A. F.; Greenbaum, J. A.; Peters, B.; Krammer, F.; Smith, D. M.; Crotty, S.; Sette, A. Targets of T Cell Responses to SARS-CoV-2 Coronavirus in Humans with COVID-19 Disease and Unexposed Individuals. *Cell* **2020**, *181* (7), 1489−1501.

(11) Ndwandwe, D.; Wiysonge, C. S. COVID-19 Vaccines. *Curr. Opin. Immunol.* **2021**, *71*, 111−116.

(12) Yadvinder, S. A.; Dinesh, S. B. a. S. K. M. Adenoviral Vector Immunity: Its Implications and Circumvention Strategies. *Curr. Gene Ther.* **2011**, *11* (4), 307−320.

(13) Weng, Y.; Li, C.; Yang, T.; Hu, B.; Zhang, M.; Guo, S.; Xiao, H.; Liang, X.-J.; Huang, Y. The Challenge and Prospect of mRNA Therapeutics Landscape. *Biotechnol. Adv.* **2020**, *40*, 107534.

(14) Iqbal, S.; Blenner, M.; Alexander-Bryant, A.; Larsen, J. Polymersomes for Therapeutic Delivery of Protein and Nucleic Acid Macromolecules: From Design to Therapeutic Applications. *Biomacromolecules* **2020**, *21* (4), 1327−1350.

(15) Halperin, A. Polymeric *vs.* Monomeric Amphiphiles: Design Parameters. *J. Macromol. Sci., Polym. Rev.* **2006**, *46* (2), 173−214.

(16) Discher, B. M.; Won, Y.-Y.; Ege, D. S.; Lee, J. C. M.; Bates, F. S.; Discher, D. E.; Hammer, D. A. Polymersomes: Tough Vesicles Made from Diblock Copolymers. *Science* **1999**, *284* (5417), 1143−1146.
(17) Rideau, E.; Dimova, R.; Schwille, P.; Wurm, F. R.; Landfester, K. Liposomes and Polymersomes: A Comparative Review Towards Cell Mimicking. *Chem. Soc. Rev.* **2018**, *47* (23), 8572−8610.
(18) Moon, J. J.; Suh, H.; Bershteyn, A.; Stephan, M. T.; Liu, H.; Huang, B.; Sohail, M.; Luo, S.; Ho Um, S.; Khant, H.; Goodwin, J. T.; Ramos, J.; Chiu, W.; Irvine, D. J. Interbilayer-Crosslinked Multilamellar Vesicles as Synthetic Vaccines for Potent Humoral and Cellular Immune Responses. *Nat. Mater.* **2011**, *10* (3), 243−251.
(19) Scott, E. A.; Stano, A.; Gillard, M.; Maio-Liu, A. C.; Swartz, M. A.; Hubbell, J. A. Dendritic Cell Activation and T Cell Priming With Adjuvant- and Antigen-Loaded Oxidation-Sensitive Polymersomes. *Biomaterials* **2012**, *33* (26), 6211−6219.
(20) Stano, A.; Scott, E. A.; Dane, K. Y.; Swartz, M. A.; Hubbell, J. A. Tunable T Cell Immunity towards a Protein Antigen Using Polymersomes *vs.* Solid-Core Nanoparticles. *Biomaterials* **2013**, *34* (17), 4339−4346.
(21) Matoori, S.; Leroux, J.-C. Twenty-Five Years of Polymersomes: Lost in Translation? *Mater. Horiz.* **2020**, *7* (5), 1297−1309.
(22) Khan, A. K.; Ho, J. C. S.; Roy, S.; Liedberg, B.; Nallani, M. Facile Mixing of Phospholipids Promotes Self-Assembly of Low-Molecular-Weight Biodegradable Block Co-Polymers into Functional Vesicular Architectures. *Polymers* **2020**, *12* (4), 979.
(23) Frank, S.; Kammerer, R. A; Mechling, D.; Schulthess, T.; Landwehr, R.; Bann, J.; Guo, Y.; Lustig, A.; Bachinger, H. P.; Engel, J. Stabilization of Short Collagen-Like Triple Helices by Protein Engineering. *J. Mol. Biol.* **2001**, *308* (5), 1081−1089.
(24) Graham, B.; McLellan, J.; Ward, A.; Kirchdoerfer, R.; Cottrell, C.; Joyce, M. G.; Kanekiyo, M.; Wang, N.; Pallesen, J.; Yassine, H.; Turner, H.; Corbett, K. *Prefusion Coronavirus Spike Proteins and Their Use*. US 2020/0061185 A1, Feb 27, 2020.
(25) Graham, B.; McLellan, J.; Ward, A.; Cottrell, C.; Joyce, M. G.; Kanekiyo, M.; Wang, N.; Pallesen, J.; Yassine, H.; Turner, H.; Kirchdoerfer, R.; Corbett, K. Prefusion Coronavirus Spike Proteins and Their Use. WO/2018/081318 A1, May 3, 2018.
(26) Barnes, C. O.; Jette, C. A.; Abernathy, M. E.; Dam, K.-M. A.; Esswein, S. R.; Gristick, H. B.; Malyutin, A. G.; Sharaf, N. G.; Huey-Tubman, K. E.; Lee, Y. E.; Robbiani, D. F.; Nussenzweig, M. C.; West, A. P.; Bjorkman, P. J. SARS-CoV-2 Neutralizing Antibody Structures Inform Therapeutic Strategies. *Nature* **2020**, *588* (7839), 682−687.
(27) Liu, Y.; Ning, Z.; Chen, Y.; Guo, M.; Liu, Y.; Gali, N. K.; Sun, L.; Duan, Y.; Cai, J.; Westerdahl, D.; Liu, X.; Xu, K.; Ho, K.-f.; Kan, H.; Fu, Q.; Lan, K. Aerodynamic Analysis of SARS-CoV-2 in Two Wuhan Hospitals. *Nature* **2020**, *582* (7813), 557−560.
(28) Noy-Porat, T.; Makdasi, E.; Alcalay, R.; Mechaly, A.; Levy, Y.; Bercovich-Kinori, A.; Zauberman, A.; Tamir, H.; Yahalom-Ronen, Y.; Israeli, M. a.; Epstein, E.; Achdout, H.; Melamed, S.; Chitlaru, T.; Weiss, S.; Peretz, E.; Rosen, O.; Paran, N.; Yitzhaki, S.; Shapira, S. C.; Israely, T.; Mazor, O.; Rosenfeld, R. A Panel of Human Neutralizing mAbs Targeting SARS-CoV-2 Spike at Multiple Epitopes. *Nat. Commun.* **2020**, *11* (1), 4303.
(29) Brouwer, P. J. M.; Caniels, T. G.; van der Straten, K.; Snitselaar, J. L.; Aldon, Y.; Bangaru, S.; Torres, J. L.; Okba, N. M. A.; Claireaux, M.; Kerster, G.; Bentlage, A. E. H.; van Haaren, M. M.; Guerra, D.; Burger, J. A.; Schermer, E. E.; Verheul, K. D.; van der Velde, N.; van der Kooi, A.; van Schooten, J.; van Breemen, M. J.; Bijl, T. P. L.; Sliepen, K.; Aartse, A.; Derking, R.; Bontjer, I.; Kootstra, N. A.; Wiersinga, W. J.; Vidarsson, G.; Haagmans, B. L.; Ward, A. B.; de Bree, G. J.; Sanders, R. W.; van Gils, M. J. Potent Neutralizing Antibodies from COVID-19 Patients Define Multiple Targets of Vulnerability. *Science* **2020**, *369* (6504), 643−650.
(30) Poh, C. M.; Carissimo, G.; Wang, B.; Amrun, S. N.; Lee, C. Y.-P.; Chee, R. S.-L.; Fong, S.-W.; Yeo, N. K.-W.; Lee, W.-H.; Torres-Ruesta, A.; Leo, Y.-S.; Chen, M. I. C.; Tan, S.-Y.; Chai, L. Y. A.; Kalimuddin, S.; Kheng, S. S. G.; Thien, S.-Y.; Young, B. E.; Lye, D. C.; Hanson, B. J.; Wang, C.-I.; Renia, L.; Ng, L. F. P. Two Linear Epitopes on the SARS-CoV-2 Spike Protein That Elicit Neutralising Antibodies in COVID-19 Patients. *Nat. Commun.* **2020**, *11* (1), 2806.
(31) Sekine, T.; Perez-Potti, A.; Rivera-Ballesteros, O.; Strålin, K.; Gorin, J.-B.; Olsson, A.; Llewellyn-Lacey, S.; Kamal, H.; Bogdanovic, G.; Muschiol, S.; Wullimann, D. J.; Kammann, T.; Emgård, J.; Parrot, T.; Folkesson, E.; Akber, M.; Berglin, L.; Bergsten, H.; Brighenti, S.; Brownlie, D.; et al. Robust T Cell Immunity in Convalescent Individuals with Asymptomatic or Mild COVID-19. *Cell* **2020**, *183* (1), 158−168.
(32) Mahajan, S.; Kode, V.; Bhojak, K.; Karunakaran, C.; Lee, K.; Manoharan, M.; Ramesh, A.; Hv, S.; Srivastava, A.; Sathian, R.; Khan, T.; Kumar, P.; Gupta, R.; Chakraborty, P.; Chaudhuri, A. Immunodominant T-Cell Epitopes from the SARS-CoV-2 Spike Antigen Reveal Robust Pre-Existing T-Cell Immunity in Unexposed Individuals. *Sci. Rep.* **2021**, *11* (1), 13164.
(33) Ou, X.; Liu, Y.; Lei, X.; Li, P.; Mi, D.; Ren, L.; Guo, L.; Guo, R.; Chen, T.; Hu, J.; Xiang, Z.; Mu, Z.; Chen, X.; Chen, J.; Hu, K.; Jin, Q.; Wang, J.; Qian, Z. Characterization of Spike Glycoprotein of SARS-CoV-2 on Virus Entry and Its Immune Cross-Reactivity with SARS-CoV. *Nat. Commun.* **2020**, *11* (1), 1620.
(34) Graham, B. S. Rapid COVID-19 Vaccine Development. *Science* **2020**, *368* (6494), 945−946.
(35) de Alwis, R.; Chen, S.; Gan, E. S.; Ooi, E. E. Impact of Immune Enhancement on Covid-19 Polyclonal Hyperimmune Globulin Therapy and Vaccine Development. *EBioMedicine* **2020**, *55*, 102768.
(36) Fulginiti, V. A.; Eller, J. J.; Downie, A. W.; Kempe, C. H. Altered Reactivity to Measles Virus: Atypical Measles in Children Previously Immunized With Inactivated Measles Virus Vaccines. *JAMA* **1967**, *202* (12), 1075−1080.
(37) Kim, H. W.; Canchola, J. G.; Brandt, C. D.; Pyles, G.; Chanock, R. M.; Jensen, K.; Parrott, R. H. Respiratory Syncytial Virus Disease in Infants Despite Prior Administration of Antigenic Inactivated Vaccine. *Am. J. Epidemiol.* **1969**, *89* (4), 422−434.
(38) Kim, S.-Y.; Lee, S.-J.; Kim, J.-K.; Choi, H.-G.; Lim, S.-J. Optimization and Physicochemical Characterization of a Cationic Lipid-Phosphatidylcholine Mixed Emulsion Formulated as a Highly Efficient Vehicle That Facilitates Adenoviral Gene Transfer. *Int. J. Nanomed.* **2017**, *12*, 7323−7335.
(39) Keswani, R. K.; Pozdol, I. M.; Pack, D. W. Design of Hybrid Lipid/Retroviral-Like Particle Gene Delivery Vectors. *Mol. Pharmaceutics* **2013**, *10* (5), 1725−1735.
(40) Jiang, X.; Lu, C.; Tang, M.; Yang, Z.; Jia, W.; Ma, Y.; Jia, P.; Pei, D.; Wang, H. Nanotoxicity of Silver Nanoparticles on HEK293T Cells: A Combined Study Using Biomechanical and Biological Techniques. *ACS Omega* **2018**, *3* (6), 6770−6778.
(41) Dress, R. J.; Wong, A. Y. W.; Ginhoux, F. Homeostatic Control of Dendritic Cell Numbers and Differentiation. *Immunol. Cell Biol.* **2018**, *96* (5), 463−476.
(42) Anderson, D. A.; Dutertre, C.-A.; Ginhoux, F.; Murphy, K. M. Genetic Models of Human and Mouse Dendritic Cell Development and Function. *Nat. Rev. Immunol.* **2021**, *21*, 101115.
(43) Merad, M.; Sathe, P.; Helft, J.; Miller, J.; Mortha, A. The Dendritic Cell Lineage: Ontogeny and Function of Dendritic Cells and Their Subsets in the Steady State and the Inflamed Setting. *Annu. Rev. Immunol.* **2013**, *31* (1), 563−604.
(44) Jia, J.; Zhang, Y.; Xin, Y.; Jiang, C.; Yan, B.; Zhai, S. Interactions between Nanoparticles and Dendritic Cells: From the Perspective of Cancer Immunotherapy. *Front. Oncol.* **2018**, *8*(404), DOI: 10.3389/fonc.2018.00404.
(45) Tian, L.; Li, X.; Qi, F.; Tang, Q.-Y.; Tang, V.; Liu, J.; Li, Z.; Cheng, X.; Li, X.; Shi, Y.; Liu, H.; Tang, L.-H. Harnessing Peak Transmission around Symptom Onset For Non-Pharmaceutical Intervention and Containment of the COVID-19 Pandemic. *Nat. Commun.* **2021**, *12* (1), 1147.
(46) Yu, P.; Yan, J.; Wu, W.; Tao, X.; Lu, X.; Liu, S.; Zhu, W. A CpG Oligodeoxynucleotide Enhances the Immune Response to Rabies Vaccination in Mice. *Virol. J.* **2018**, *15* (1), 174.
(47) Kuo, T.-Y.; Lin, M.-Y.; Coffman, R. L.; Campbell, J. D.; Traquina, P.; Lin, Y.-J.; Liu, L. T.-C.; Cheng, J.; Wu, Y.-C.; Wu, C.-C.; Tang, W.-

H.; Huang, C.-G.; Tsao, K.-C.; Chen, C. Development of CpG-Adjuvanted Stable Prefusion SARS-CoV-2 Spike Antigen as a Subunit Vaccine against COVID-19. *Sci. Rep.* **2020**, *10* (1), 20085.
(48) Diwan, M.; Elamanchili, P.; Cao, M.; Samuel, J. Dose Sparing of CpG Oligodeoxynucleotide Vaccine Adjuvants by Nanoparticle Delivery. *Curr. Drug Delivery* **2004**, *1* (4), 405−412.
(49) Nie, J.; Li, Q.; Wu, J.; Zhao, C.; Hao, H.; Liu, H.; Zhang, L.; Nie, L.; Qin, H.; Wang, M.; Lu, Q.; Li, X.; Sun, Q.; Liu, J.; Fan, C.; Huang, W.; Xu, M.; Wang, Y. Establishment and Validation of a Pseudovirus Neutralization Assay for SARS-CoV-2. *Emerging Microbes Infect.* **2020**, *9* (1), 680−686.
(50) Hoffmann, M.; Kleine-Weber, H.; Schroeder, S.; Krüger, N.; Herrler, T.; Erichsen, S.; Schiergens, T. S.; Herrler, G.; Wu, N.-H.; Nitsche, A.; Müller, M. A.; Drosten, C.; Pöhlmann, S. SARS-CoV-2 Cell Entry Depends on ACE2 and TMPRSS2 and Is Blocked by a Clinically Proven Protease Inhibitor. *Cell* **2020**, *181* (2), 271−280.
(51) Johnson, M. C.; Lyddon, T. D.; Suarez, R.; Salcedo, B.; LePique, M.; Graham, M.; Ricana, C.; Robinson, C.; Ritter, D. G. Optimized Pseudotyping Conditions for the SARS-COV-2 Spike Glycoprotein. *J. Virol.* **2020**, *94* (21), e01062−20.
(52) Jiang, S.; Hillyer, C.; Du, L. Neutralizing Antibodies against SARS-CoV-2 and Other Human Coronaviruses. *Trends Immunol.* **2020**, *41* (5), 355−359.
(53) Kim, C.; Fang, F.; Weyand, C. M.; Goronzy, J. J. The Life Cycle of a T Cell after Vaccination − Where Does Immune Ageing Strike? *Clin. Exp. Immunol.* **2017**, *187* (1), 71−81.
(54) Corbett, K. S.; Edwards, D.; Leist, S. R.; Abiona, O. M.; Boyoglu-Barnum, S.; Gillespie, R. A.; Himansu, S.; Schäfer, A.; Ziwawo, C. T.; DiPiazza, A. T.; Dinnon, K. H.; Elbashir, S. M.; Shaw, C. A.; Woods, A.; Fritch, E. J.; Martinez, D. R.; Bock, K. W.; Minai, M.; Nagata, B. M.; Hutchinson, G. B.; et al. SARS-CoV-2 mRNA Vaccine Development Enabled by Prototype Pathogen Preparedness. *bioRxiv* **2020**, 06.11.145920.
(55) Iwasaki, A.; Medzhitov, R. Toll-Like Receptor Control of the Adaptive Immune Responses. *Nat. Immunol.* **2004**, *5* (10), 987−995.
(56) Ma, D. Y.; Clark, E. A. The Role of CD40 and CD154/CD40L in Dendritic cells. *Semin. Immunol.* **2009**, *21* (5), 265−272.
(57) Hubo, M.; Trinschek, B.; Kryczanowsky, F.; Tüttenberg, A.; Steinbrink, K.; Jonuleit, H. Costimulatory Molecules on Immunogenic *versus* Tolerogenic Human Dendritic Cells. *Front. Immunol.* **2013**, *4*, 82.
(58) Dalod, M.; Chelbi, R.; Malissen, B.; Lawrence, T. Dendritic Cell Maturation: Functional Specialization through Signaling Specificity and Transcriptional Programming. *EMBO J.* **2014**, *33* (10), 1104−1116.
(59) Weeratna, R. D.; Brazolot Millan, C. L.; McCluskie, M. J.; Davis, H. L. CpG ODN Can Re-Direct the Th Bias of Established Th2 Immune Responses in Adult and Young Mice. *FEMS Immunol. Med. Microbiol.* **2001**, *32* (1), 65−71.
(60) Balkovic, E. S.; Florack, J. A.; Six, H. R. Immunoglobulin G Subclass Antibody Responses of Mice to Influenza Virus Antigens Given in Different Forms. *Antiviral Res.* **1987**, *8* (3), 151−160.
(61) Coutelier, J. P.; van der Logt, J. T.; Heessen, F. W.; Warnier, G.; Van Snick, J. IgG2a Restriction of Murine Antibodies Elicited by Viral Infections. *J. Exp. Med.* **1987**, *165* (1), 64−69.
(62) Knudson, C. J.; Hartwig, S. M.; Meyerholz, D. K.; Varga, S. M. RSV Vaccine-Enhanced Disease Is Orchestrated by the Combined Actions of Distinct CD4 T Cell Subsets. *PLoS Pathog.* **2015**, *11* (3), No. e1004757.
(63) Long, Q.-X.; Tang, X.-J.; Shi, Q.-L.; Li, Q.; Deng, H.-J.; Yuan, J.; Hu, J.-L.; Xu, W.; Zhang, Y.; Lv, F.-J.; Su, K.; Zhang, F.; Gong, J.; Wu, B.; Liu, X.-M.; Li, J.-J.; Qiu, J.-F.; Chen, J.; Huang, A.-L. Clinical and Immunological Assessment of Asymptomatic SARS-CoV-2 Infections. *Nat. Med.* **2020**, *26* (8), 1200−1204.
(64) Le Bert, N.; Tan, A. T.; Kunasegaran, K.; Tham, C. Y. L.; Hafezi, M.; Chia, A.; Chng, M. H. Y.; Lin, M.; Tan, N.; Linster, M.; Chia, W. N.; Chen, M. I. C.; Wang, L.-F.; Ooi, E. E.; Kalimuddin, S.; Tambyah, P. A.; Low, J. G.-H.; Tan, Y.-J.; Bertoletti, A. SARS-CoV-2-Specific T Cell Immunity in Cases of COVID-19 and SARS, and Uninfected controls. *Nature* **2020**, *584* (7821), 457−462.
(65) Khoury, D. S.; Cromer, D.; Reynaldi, A.; Schlub, T. E.; Wheatley, A. K.; Juno, J. A.; Subbarao, K.; Kent, S. J.; Triccas, J. A.; Davenport, M. P. Neutralizing Antibody Levels Are Highly Predictive of Immune Protection From Symptomatic SARS-CoV-2 Infection. *Nat. Med.* **2021**, *27* (7), 1205−1211.
(66) Ko, J.-H.; Joo, E.-J.; Park, S.-J.; Baek, J. Y.; Kim, W. D.; Jee, J.; Kim, C. J.; Jeong, C.; Kim, Y.-J.; Shon, H. J.; Kang, E.-S.; Choi, Y. K.; Peck, K. R. Neutralizing Antibody Production in Asymptomatic and Mild COVID-19 Patients, in Comparison with Pneumonic COVID-19 Patients. *J. Clin. Med.* **2020**, *9* (7), 2268.
(67) Sadarangani, M.; Marchant, A.; Kollmann, T. R. Immunological Mechanisms of Vaccine-Induced Protection against COVID-19 in Humans. *Nat. Rev. Immunol.* **2021**, *21* (8), 475−484.
(68) Mohsen, M. O.; Gomes, A. C.; Cabral-Miranda, G.; Krueger, C. C.; Leoratti, F. M. S.; Stein, J. V.; Bachmann, M. F. Delivering Adjuvants and Antigens in Separate Nanoparticles Eliminates the Need of Physical Linkage for Effective Vaccination. *J. Controlled Release* **2017**, *251*, 92−100.
(69) Lip, K.-M.; Shen, S.; Yang, X.; Keng, C.-T.; Zhang, A.; Oh, H.-L. J.; Li, Z.-H.; Hwang, L.-A.; Chou, C.-F.; Fielding, B. C.; Tan, T. H. P.; Mayrhofer, J.; Falkner, F. G.; Fu, J.; Lim, S. G.; Hong, W.; Tan, Y.-J. Monoclonal Antibodies Targeting the HR2 Domain and the Region Immediately Upstream of the HR2 of the S Protein Neutralize *in Vitro* Infection of Severe Acute Respiratory Syndrome Coronavirus. *J. Virol.* **2006**, *80* (2), 941−950.

https://doi.org/10.1021/acsnano.1c01243
ACS Nano 2021, 15, 15754−15770